Single Photon Detection and Timing: Experiments and Techniques

SHERMAN K. POULTNEY

Department of Physics and Astronomy,
University of Maryland,
College Park, Maryland

I. Introduction

Single photon detection and timing means essentially the detection and timing of a single photoelectron released by light from a photosensitve surface of a photomultiplier, channel multiplier, avalanche multiplier photodiode, or other photodevice. An electron released by a particle or photon bombardment of a windowless multiplier is also thus included. Single photoelectron detection requires sufficient low noise amplification to overcome the Johnson noise in the first resistor of the eventual electronic circuit plus additional amplification to operate standard discriminator detection circuits. The time response is usually quite fast due to the desire to count at both low and high rates, to time closely spaced events, or to time intervals to highest precision,

and so most of the gain usually comes before the electronic circuits. This gain is obtained by secondary electron emission processes or their equivalent down a chain of electrodes or a continuous channel and is subject to statistical fluctuations. The resultant fluctuations in the output charge can affect timing with single photoelectron pulses, the length of time needed to achieve a light flux measurement to a given precision, the efficiency of single photoelectron detection, and the discrimination against some types of device noise. The major type of device noise has a similar output charge distribution, however, and this dark noise must be reduced by cooling the photodevice or by other techniques in most weak light applications. Background light noise also has a similar distribution and must be reduced when present by narrow spectral and spatial filters. Correct technique can help minimize device noise, but is often neglected. It is important to have standard experimental tests to evaluate the single photon counting performance and the noise performance of photodevices.

Use of certain photoemissive materials and reduced photosurface size can also reduce device noise. However, for single photon counting, the choice of material is usually dictated by quantum efficiency considerations at the wavelength of interest. A number of opaque, reflection-mode photosurfaces are now available which extend the spectral range of high sensitivity. The older transmission-type photosurfaces show worthwhile increases in sensitivity by means of external and internal quantum efficiency enhancement techniques. The total quantum counting efficiency of a photodevice can often be lower than the photosurface quantum efficiency. The discrepancy may be caused by those photoelectrons that fail to get collected by the multiplier or by those anode pulses that fail to exceed the discriminator threshold due to the multiplication statistics. A low counting efficiency is just as serious as a low photosurface quantum efficiency and should be evaluated for any photodevice under consideration. Experiments involving single photon detection are usually photometric or spectrophotometric measurements of a weak light beam. The weak intensity may be due to scattering with small cross sections as in laboratory studies of Raman and Brillouin lineshifts or due to weak astronomical sources being viewed directly or through a many-channel spectrophotometer. The length of time needed to obtain a given precision is limited by background noise, device noise, or signal shot noise depending on which cannot be reduced. Digital storage of standardized discriminator pulses has both theoretical and practical advantages over other storage and detection methods. If the light source can be effectively modulated, digital synchronous detection can be used at least for convenience and stability in much the same manner as analog synchronous detection. If photometry over a wide range of intensities is required, the single photon counting method will be limited by photodevice or circuit time responses or dead times.

A second class of experiments requires both single photon detection and precise (nanosecond or better) timing. Timing of this precision depends on both the photodevice and the arrival time detection circuit. The photodevice must be designed to minimize electron transit time spreads; especially between the photosurface and multiplier and in the first stages of the multiplier. The timing capabilities and limitations of some representative photomultipliers are examined closely in order to understand the timing capabilities and limitations of improved photomultipliers and other new photodevices. The arrival time detection circuit should be of the constant-fraction-of-pulse-height type or its equivalent to minimize any timing spread due to the multiplication fluctuations of the photodevice output signal. A photodevice which itself reduces these fluctuations in some manner also helps to minimize this time walk. A short time interval between two events of interest is best measured by sending the now standard timing pulses to a time-to-pulse-height converter which can be interrogated by a suitable analog-to-digital converter. The time distribution of intervals between repeatable physical events can be stored in a multichannel pulse height analyzer for on-line or later use. If the time interval becomes too long to obtain the desired resolution with a time-to-pulse-height converter, either the time-to-pulse-height converter has to be used in conjunction with a suitable digital time-interval meter or another timing method must be used. Methods for measuring the timing precision and accuracy of photodevices with single photons are outlined with special emphasis on the necessary fast light pulses. Methods of calibrating and monitoring the stability of the timing circuits are also outlined. Typical photon timing experiments are the measurement of atomic and molecular fast fluorescence decay times and the lunar ranging experiment. The former measurement often has plenty of light signal, but this signal is attenuated to single photon levels in order to measure the fast decay time statistically so that it is limited only by the photodevice transit time spread. The width of any short light pulse can similarly be examined. Reference to the large body of work at higher light levels with scintillators is made since this work sets the basis for the terminology, theory, and past performance of photodevices for fast timing. In the lunar ranging experiment, the very low signal cannot be significantly increased. In spite of the high signal attenuation, high background noise, and difficult pointing problem, nanosecond timing of a 2.5 sec interval is now being done at the single photon level with current nanosecond laser transmitters. Ultrashort pulse lasers will leave the photodevice as the limiting factor in achieving the goals of that experiment.

A third class of experiments requires single photon detection in addition to moderate timing capabilities. The time information may be added to the light signal by effectively modulating it in order to employ synchronous detection to aid in the separation of signal from noise. Optical radar is a

pulsed version of this modulation and can be used for probing of the structure of the atmosphere, for example. The measurement of the arrival time distribution of photons in a light beam can characterize the statistical properties of that light beam. If the beam properties are known, this measurement on scattered light can yield information about the internal behavior of a scattering medium undergoing statistical fluctuations in some property. These fluctuations may be due to particles undergoing Brownian movement in a liquid or to driven or spontaneous excitations of the medium. The spontaneous thermal excitations can be either propagating as in the case of optical and acoustic phonons which yield Raman and Brillouin scattering, respectively, or nonpropagating as in the case of density fluctuations at constant pressure which yield Rayleigh scattering. The measurement of photon arrival time is thus a valuable complement to spectroscopic studies of the above phenomena in that it is able to resolve the narrow linewidths. Typical experiments considered are the study of particles in Brownian motion and the measurement of the statistical properties of a narrowband thermal light source. The question of time-correlated photodevice noise can be studied with these same techniques.

All of the above topics about single photon detection and timing cannot be treated in detail here. Wherever possible, reference is made to current reviews in the literature about individual topics. It is hoped that the following introduction will allow new workers to use these techniques in their fields of interest and will provide old hands with a current survey of the field which integrates many loose ends.

II. Single Photon Detection

A. Necessary Photodevice Gain and Detection Circuits

Consider an electron produced by photoemission from the photosurface of a photodevice (e.g. Fig. 1). This electron must be detected by electronic circuits in order to be of further use. It constitutes a charge pulse of 1.6×10^{-19} C. Such a charge pulse is often collected on an RC network between photodevice anode and detection circuit. To be detected, the corresponding voltage pulse must exceed some preset level in the integral pulse height discriminator or single channel pulse height analyzer which then generates a standard counting pulse (*1*). If the time constant of the RC network can be much greater than the photodevice impulse response time, then the peak of the corresponding voltage pulse

$$V_p = e/C \tag{1}$$

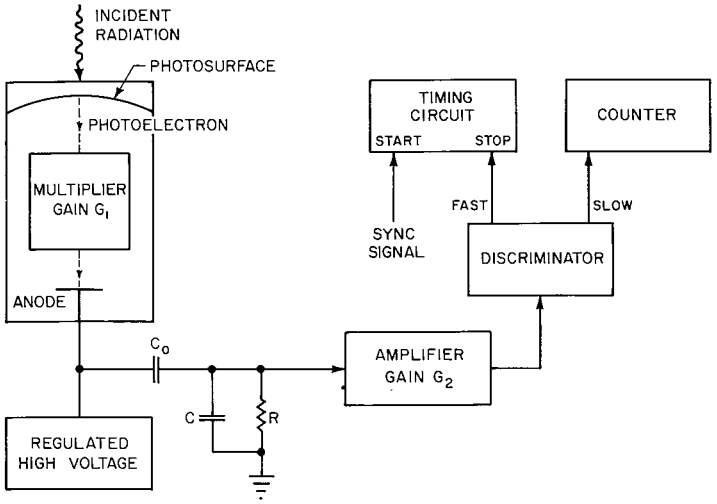

FIG. 1. Schematic of single photon detection and timing with a photomultiplier. Diagram is not to scale. C_0 is bypass capacitor used when anode is at high potential.

which is a measure of the total charge of the charge pulse. In this case, V_p would equal 25 nV if C is taken be the stray capacitance $40/2\pi$ pF and certainly needs amplification to be detected. The amplification must be of a special kind because charge fluctuations in the output resistance, R, of the photodevice due to Johnson noise will be the basic limitation to detection. These spontaneous charge fluctuations in R at a temperature T yield a voltage fluctuation for the RC network given by

$$(V^2)_{\text{rms}} = (kT/e)(e/C) \tag{2}$$

where $k = 1.38 \times 10^{-23}$ J/°K. In order for the emitted photoelectron to be detected above Johnson noise during the observation time, it must be amplified without the use of a resistance by a charge gain G_1 such that it is larger than the fluctuation charge. The necessary G_1 is thus given by

$$G_1^2 \geq (C/e)(kT/e), \tag{3}$$

where kT/e equals 0.025 V at 300°K. In the present case, G_1 must be greater than 10^4 which yields a voltage pulse with a peak of 0.25 mV. An additional gain G_2 of at least 200 is needed to activate the discriminator. This gain can be provided by an amplifier for slow counting applications. Kowalski (*1*) discusses the many aspects of amplification, pulse-shaping, and detection. Both the RC integration method and slow electronics were developed for precise measurements of the total charge contained in the anode pulse and for operation with counting dead times of about 1 μsec.

The need to count at higher rates or to time short intervals makes it necessary to treat the photodevice anode pulse in a different manner. Neither single photon detection nor timing requires a precise measurement of charge. The RC time constant of the output circuit can then be made less than or equal to the pulse width or circuit resolution time whichever is longer. If the device is already being operated to minimize C, the time constant can only be lowered by decreasing R. The peak of the voltage pulse across RC now becomes lower than that given by (1) because it corresponds to less than the total charge. The gain of the device G_1 must be raised to overcome the Johnson noise. For example, a good approximation for the anode current pulse of a photomultiplier is given by

$$i(t) = i_p \exp[-(t-h)^2/2\lambda^2] = (G_1 e/\sqrt{2\pi}\lambda) \exp[-(t-h)^2/2\lambda^2], \quad (4)$$

where the full width of the current pulse at half-maximum is given by 2.36 λ and where h is the average transit time in the device. The voltage pulse across R of the network of Fig. 1 can be obtained with some reinterpretation from the work of Lewis and Wells (*2*).

$$V(t) = \frac{Ge}{2C} \exp\left[\frac{-(t-h)}{RC} + \frac{\lambda^2}{2RC}\right] \left\{ \operatorname{erf}\left[\frac{(t-h)}{\sqrt{2}\,\lambda} - \frac{\lambda}{\sqrt{2}\,RC}\right] + \operatorname{erf}\left[\frac{h}{\sqrt{2}\,\lambda} + \frac{\lambda}{\sqrt{2}\,RC}\right]\right\}. \quad (5)$$

If $V(t)$ is expressed as

$$V(t) = (G_1 e/C) D(t, h, \lambda, RC), \quad (6)$$

one can display the solutions as in Fig. 2 for several λ/RC ratios. Note well the units along the abscissa. This unorthodox scale allows either λ or RC to

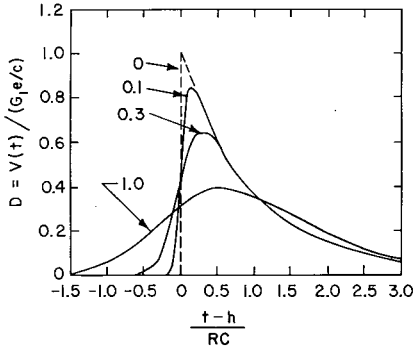

FIG. 2. Voltage waveform from RC network of Fig. 1 corresponding to a Gaussian current pulse from photomultiplier anode. Parameter is $\sqrt{2}\,\lambda/RC$. Figure after Fig. 7.3 of Lewis and Wells (*2*). (Courtesy of Pergamon Press.)

be varied. For $RC = \sqrt{2}\,\lambda$, the peak voltage is 0.4 of that in (1) and G_1 must be 2.5×10^4 for detection above Johnson noise. A typical λ for a fast photomultiplier is about 1 nsec (i.e. full width of 2.4 nsec) so that if $RC = \sqrt{2}\,\lambda$ the R equals 220 Ω for the above stray capacitance C. Standard fast detection circuitry is usually based on 50 Ω so that G_1 must be 10^5 or greater for fast detection of single photoelectrons above the Johnson noise. The standard fast integral discriminators or timing discriminators typically have thresholds of 50 mV so that the additional G_2 of at least 200 is still needed. For fast counting (e.g. 100 MHz), this G_2 may be provided by a fast amplifier. For precise timing, it is essential that the whole gain be provided by G_1 of the photodevice, which here must be 2×10^7. Discussion of the necessary fast circuits can be found in Kowalski (*1*), Meiling and Stary (*3*), or the product literature. Precise timing with photodevices is considered in Section III. Other constraints on single photodetection and photometric measurements are discussed here in Section II.

The above gain considerations are important when examining the suitability of new photodevices for single photon detection. They are also important as a guide to the redesign of present devices. In trying to improve count rates and timing capabilities of photomultipliers, designers now try to reduce λ and, concomitantly, the stray capacitance C since R is probably fixed. The former is done by electrode and field design. The latter is accomplished by the use of a coaxial structure for the anode output which also reduces pulse distortion by eliminating electrical discontinuities (*4*). These reductions lead to a corresponding decrease in the necessary gain by (4) as long as the detection circuits are fast enough. Some photodevices may be subject to cooling along with the resistance R and so would also have a lower gain requirement since the Johnson noise is lowered by (2). Operation of many photomultipliers at high gain can lead to noise problems as discussed in Section II,C. Some photodevices are subject to gain nonlinearities under certain conditions. In a photomultiplier, the gain is subject to saturation caused by the basic limitation of space charge effects in the final stages (*5,6*). This gain saturation limits the peak anode current. An increase in the applied high voltage then increases the total charge gain and so broadens the pulse width. If gain saturation is reached before the level of single photon detection, one can sacrifice speed for gain by using an amplifier G_2 in conjunction with a lower G_1 or by using a larger RC. If sufficient gain G_1 is available and maximum count rates are not required, saturation may have a beneficial effect on timing precision as mentioned in Section III,B. At high gains there is also the danger that the high peak or average currents can damage the electrodes of the photomultiplier. The above and other photomultiplier nonlinearities as well as corrective procedures are discussed by Kowalski (*1*), Pietri and Nussli (*5*), and RCA Staff (*4*).

B. Mechanisms and Statistics of Photodevice Gain

1. Introduction

Photodevice gains up to 10^9 can be attained without the use of a resistance by means of secondary electron emission. If a photoelectron from the photosurface in Fig. 3 is given sufficient kinetic energy before striking an electrode,

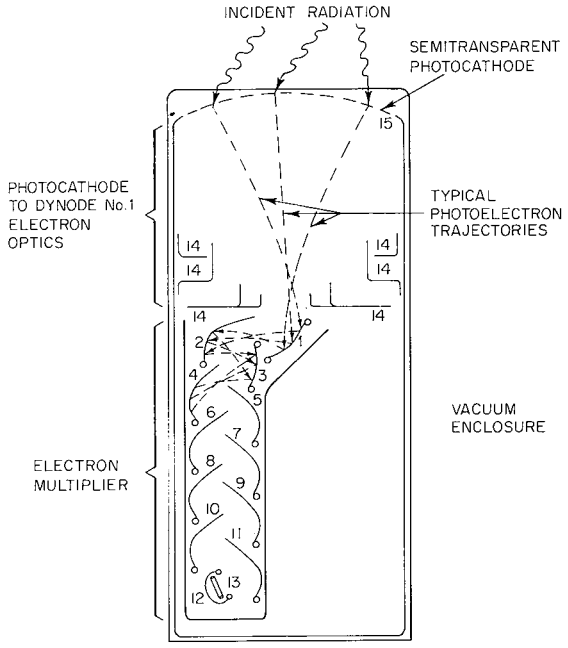

FIG. 3. Schematic of a typical photomultiplier employing a focused multiplier. Electrodes 1–12 are dynodes, 13 is anode, 14 are focusing electrodes, and 15 is the photocathode. Some electron trajectories are shown. RCA Staff (*4*). (Courtesy of RCA.)

a number g of electrons will be emitted from that electrode. A chain of these multiplications can be arranged at separate electrodes as in Fig. 3 for a photomultiplier or along the continuous surface of a curved channel as for a channel multiplier if the cascading charge packet is suitably directed. The time response of the photodevice depends on the secondary electron trajectories, their energy distribution, and their spatial distribution; the multiplication at each electrode; and the number of multiplication steps. These limitations to time responses in the nanosecond region are discussed in Section III,A. A solid-state analog of the secondary gain of a multiplier is being developed in

the form of a carrier avalanche process in semiconductor diodes (*7*). Gains of 10^2 to 10^4 have been reached in small area diodes (*8*).

If the electron multiplier were an ideal device, the anode output pulses resulting from single photoelectrons would have exactly the same charge. However, in a real device, not only might some of the photoelectrons go uncollected by the multiplier, but the secondary emission process is a statistical process. The multiplier gain G_1 is an average gain and the multiplication factors g are average values. Output charge pulses therefore have a spectrum of sizes. These fluctuations in the output charge need not affect single photon detection as outlined in Fig. 1 as long as the spectrum is well-behaved at the lower end where the level of the integral discriminator would be set. Otherwise, a number of the smaller single photon pulses would be lost and a number of small noise pulses may be added. The pulse height spectrum can also affect system time resolution as discussed in Section III,B.

2. *Secondary Electron Emission*

Within the last few years, important improvements have been made in secondary emission (and photoemission) from materials. In order to understand these improvements and their relation to multiplication fluctuations and fast timing, a description of the emission process is given in Section II,E,2 for photoemission and the differences for secondary emission are given here. Secondary emitters are either semiconductors or insulators with a band structure similar to that in Fig. 6 (*9*). An energetic electron incident upon a secondary emitter excites a number of electrons to the conduction band. Some of these electrons move towards the surface and escape if their energies are greater than the electron affinity energy of the surface. During the transport to the surface, the electrons lose energy as a result of phonon or electron collisions. In conventional secondary emitters, one thus expects and observes the multiplication factor g to increase with the energy of the primary. However, a more energetic primary excites electrons at greater depths in the material from which escape is much less probable. Consequently, g reaches a peak at some primary energy and then decreases. This peak value is typically from 6 to 10, but at primary electron energies somewhat higher than typical for photodevice electrode potentials. The distribution in energy and direction of the secondary electrons has an important bearing on the time resolution of the photodevice as discussed in Section III,A,1. Conventional emitters have quite large spreads in energy (i.e. 1 to 10 eV) (*10*).

Improvement in secondary emission has been obtained by modifying the band structure with a surface layer of electropositive Cs on GaP as shown in Fig. 7 and as discussed in Section II,E,2. Under these conditions even the thermalized secondary electrons in the conduction band can escape the surface.

Secondary electrons thus have a much greater escape depth and the multiplication at an electrode can be expected to be much larger than for the same primary energy incident on a conventional material. Multiplications of up to 50 have been observed in production photomultipliers for a single GaP dynode (*11*). These authors also point out the expectation that the energy distribution of secondary electrons will be quite narrow with the highest energy about 1 eV. Such an energy distribution would lead to an improvement in multiplier time resolution. However, this improvement is limited by the long diffusion times (e.g. 100 psec) of excited electrons which are related to the greater escape depths.

3. Gain and Gain Statistics for Discrete Dynode Multipliers

A number of multipliers with high gain, well-focused structures (e.g. Fig. 3) have an output pulse height distribution for single photoelectrons that is peaked with a fairly narrow width. A typical single photoelectron distribution is shown in Fig. 4. These distributions can be obtained with the circuit

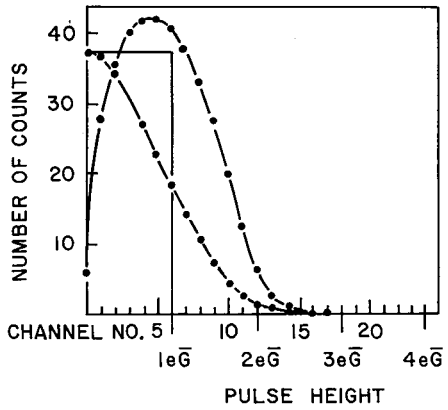

FIG. 4. Single photoelectron integral and differential pulse height distributions. RCA type 4501 (similar to 8575). Photocathode K_2CsSb. Counting time 10 min. Morton (*7*).

of Fig. 1 as discussed in Section II,D. By varying the level of the integral discriminator, one obtains the integral curve which intersects the ordinate at the total number of electrons entering the multiplier during the observation period. This integral curve allows one to calibrate the abscissa of the pulse height distribution curve in equivalent photoelectrons. Note that the spread of the distribution due to multiplication statistics causes some of the single photoelectrons to appear as doubles and others to be lost below a discriminator threshold. If the threshold could be set at the lower end of a very narrow

distribution without admitting any low amplitude device noise, one could expect stable single photon detection in spite of gain changes due to causes other than multiplication statistics.

Theoretical derivations of single electron response (i.e. SER) amplitude distribution by a number of authors are summarized by Donati, Gatti, and Svelto (*12*) with particular emphasis on scintillation spectrometry. Various stochastic processes are used as models for secondary electron emission from an individual multiplier electrode. The SER distribution is obtained from an appropriate probability generating function which cascades the distribution successively down the electrode (or dynode) chain. The mean gain of the multiplier G_1 is then the product of the mean multiplication factor g of each dynode and results in an output pulse with mean amplitude A. If a Poisson process is assumed to describe the secondary emission at a dynode and if each dynode has equal mean gain, one can compute an SER amplitude distribution that resembles Fig. 4 for a g of about 4. One can also calculate the percentage of single photoelectrons lost in the multiplication process for various g as in Table I (*13*). For $g = 4$, this loss is less than a few percent. It is often con-

TABLE I

PERCENTAGE OF SINGLE PHOTOELECTRON PULSES LOST IN A MULTIPLIER FOR DIFFERENT VALUES OF DYNODE GAIN g[a]

g	Percent lost
1.5	42
2.0	20
2.5	11
3.0	6
5.0	0.70

[a] Lombard and Martin (*13*). (Courtesy of American Institute of Physics.)

venient to use the ratio Δ of the full width of the SER amplitude distribution at half-maximum to the peak amplitude as a measure of the observed (or expected) width for a particular photomultiplier with dynode gain g. Here Δ is related to the relative variance ε_A^2 by 2.35 ε_A. The relative variance is given by Morton (*14*) as

$$\varepsilon_A^2 = g\varepsilon_g^2/(g-1) = 1/(g-1) \tag{7}$$

for a Poisson process ($\varepsilon_g^2 = 1/g$) at each dynode and for a sufficiently long chain of dynodes. Much work has gone into trying to resolve the discrepancy of observations with theory for older photomultipliers. Relative variances larger than predicted by (7) are ascribed to non-Poissonian statistics in the secondary emission process itself or to a nonuniformity of gain on a dynode surface. In either case, the gain variance of a dynode is better expressed by $\varepsilon_g^2 = (bg + 1)/g$ where b expresses the deviation from Poisson behavior. The closer b is to 1, the larger the dynode variance, the amplitude variance and the Δ. Stable and efficient single photon detection requires a photomultiplier with a fairly narrow SER amplitude distribution (i.e. $g \geq 4$).

The width of the SER amplitude distribution can be decreased in several ways. With conventional dynode materials, one can increase dynode gain to its maximum value of 6 to 10 by raising electrode potentials. Fortunately, the first dynode has a dominant influence on the ε_A^2 as might be expected and only the first dynode or two need the high potentials. By regarding the first dynode as the source of the group of g_1 electrons, one can compute the ε_A^2 for a photomultiplier with remaining dynodes of gain g and for Poisson statistics using the results of Morton (*14*).

$$\varepsilon_A^2 = g/(g - 1)g_1. \tag{8}$$

The Δ for a photomultiplier with $g_1 = 10$ and $g = 5$ would be 0.83 which is an improvement of 40% over a uniform gain photomultiplier. One can narrow the Δ much more dramatically by using the high gain dynode material on the first dynode. The Δ for a photomultiplier with $g_1 = 43$ and $g = 5$ would be 0.40 which is close to that measured by Morton, Smith, and Krall (*15*). Such a photomultiplier is an excellent device for single photon detection. It allows stable, efficient counting in addition to the capability of studying its noise behavior, as disccused in Section II,C,1. Figure 5 shows the remarkably narrow peak of the distribution for single photoelectron noise (as well as other noise).

Photomultipliers employing discrete dynodes and static, crossed electric and magnetic fields have been built to obtain fast time response as discussed in Section III,A,2. Their usefulness for single photon detection can be judged on the basis of their total gains which are 2×10^4 to 10^5 and of their dynode gains of 3 to 4.

4. Gain and Gain Statistics for Continuous Multipliers

Several varieties of continuous electron multipliers exist. Heroux (*16*) reviews the detection performance of a crossed-field continuous multiplier with respect to a discrete dynode multiplier. The crossed-field continuous multiplier uses a straight strip of high resistance dynode material. The electrons

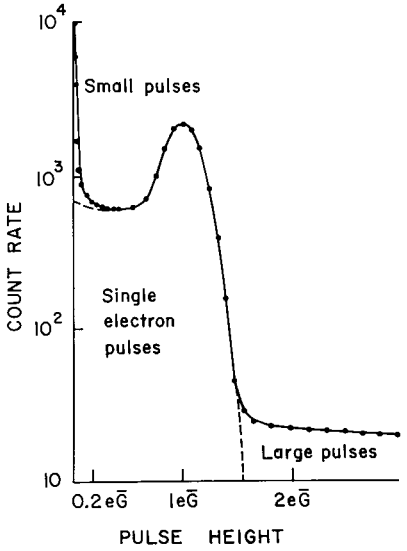

FIG. 5. Diagrammatic noise pulse height distribution. RCA type C31000D (similar to 8575 but with GaP first dynode). Single electron noise represented by dotted line. Coates (*21*). (Courtesy of The Institute of Physics.)

are guided between successive impacts on the dynode strip by means of an electric field between the dynode strip and a parallel (field) strip and by means of a crossed magnetic field. Gains high enough to detect single photoelectrons (e.g. $G_1 = 10^7$) can be obtained, but the SER amplitude distribution is very broad and lacks a well-defined peak. This distribution is attributed to a low value of dynode multiplication (e.g. $g = 1.5$) at the first impact and to an effective nonuniformity of the multiplication factor due to photoelectrons striking the dynode strip at different positions. Moreover, the percentage of single photoelectron pulses lost in the multiplier would be expected to be high (e.g. 42), from Table I. Other impediments to the use of the crossed-field magnetic multiplier for single photon detection would be additional loss in efficiency due to photoelectron collection problems between photosurface and multiplier and a regeneration noise problem.

The channel multiplier overcomes most of the above problems as described in a review by Wolber (*17*) and makes an attractive photodevice for single photon detection and timing. The channel multiplier is a hollow glass tube with a secondary-emitting coating deposited on its inner surface. Its length is relatively long compared to its inside diameter which is typically 1 mm. A voltage is applied to the ends of the channel to establish a uniform field along its axial length. An electron injected into the channel will be

accelerated down the channel until it hits the wall to begin the multiplication process. The secondaries again are accelerated and collide with the wall due to their transverse energy components. Gains of 10^7 are easily obtained. The SER amplitude distribution might be expected to be very broad from the discussion above. Such a behavior is found for moderate gains. However, at higher gains, SER amplitude distributions are obtained that are as narrow as the one in Fig. 5 for the high gain dynode photomultiplier. The cause of this narrowing is output pulse saturation. The mechanism for this saturation has been most recently studied by Harris (*18*). Stable single photon detection can thus be expected. Injection of the photoelectron into the multiplier is usually done by an accelerating potential of about 200 V so that the first multiplication factor is about 3 and only a small loss is present inside the multiplier. The channel is usually curved to minimize regeneration noise. Due to its small size, the channel multiplier has other advantages with respect to device noise and to fast timing as discussed below in Sections II,C,2 and III,A,3, respectively. The saturated output pulse is typically 10 to 20 nsec long. For single photon detection, the considerations of Section II,A indicate that load resistances of 2000 Ω or greater are optimum. The channel multiplier is limited in maximum counting rate to about 10^5 counts/sec by current limitations and not by the pulse width. However, maximum count rates up to 10^7 counts/sec have been obtained by Zatzick (*19*) using an auxiliary amplifier.

An elaboration of the channel multiplier is a bundle of channels called a wafer. One such michrochannel wafer photomultiplier is described by Boutot and Pietri (*20*). It consists of about 5×10^4 microchannels with individual diameters of 40 μm. The useful photocathode diameter was about 1 cm and the multiplier gain was about 10^5. The mircochannel wafer thus retains many of the channel multiplier advantages with the addition of a larger photosurface which is a necessity for many workers. However, the SER amplitude distribution has not yet been reported.

C. Photodevice and Background Noise and Their Reduction

It does no good to be able to detect single photons if they are obscured by background and/or photodevice noise. An ideal photodevice would probably be one in which the only noise source was thermionic emission of electrons from the photocathode. In such a case, noise photoelectrons would exhibit the same SER amplitude distribution as signal photoelectrons. The same would be true for background noise photoelectrons. The only way to separate signal from noise is then to reduce the noise to tolerable levels by an appropriate technique or by choice of an appropriate photodevice. Figure 5 shows the noise pulse height distribution of a photomultiplier. Its behavior is not ideal in that there are additional pulses both smaller and larger than the well-

defined peak of single thermal electron pulses. The narrow SER amplitude distribution here allows one to set the threshold of the integral discriminator of Fig. 1 so as to accept most of the single electron pulse and reject most of the small pulses. The causes and reduction of photodevice and background noise is discussed below. The limits that the various noise sources set to single photon detection are discussed in Sections II,G; II,C,1; and IV, both in general and for particular photodevices.

1. Device Noise in Photomultipliers and Its Reduction

Noise in photomultipliers depends greatly on the type of photomultiplier, the type of photocathode, the operating gain, technique, and the history of the particular photomultiplier selected. Attention is directed here to a recent study by Coates (*21*) of the dark noise performance of the photomultiplier with the high gain dynode discussed in Section II,B,3. The narrow SER amplitude distribution allows one to separate, identify, and study its various noise sources. Figure 5 shows a diagrammatic pulse height distribution for this photomultiplier at gains of about 10^7 when the photocathode is shielded from external light sources. The contribution from single noise electrons is indicated by the broken line. Subtraction leaves two other classes of noise; small pulses below 0.2 electrons and large pulses above 2 electrons which account for 5 to 10% of the total counts. The small pulses were attributed to three sources; thermal emission from the dynodes, internal ohmic leakage between anode and the dynodes, and electron emission from the dynodes as a result of bombardment by ions. The small pulses are of minimal importance here because they can be discriminated against with little loss in single photon detection. The large pulses were also divided into three groups; ion pulses, afterpulses, and pulses due to cosmic rays. Ion pulses are single large pulses occurring at random and are due to ion bombardment of the photocathode. They are the major source of large pulses in this photomultiplier and their count rate increases with both gain and temperature. Afterpulses are due to ions formed in the region between photocathode and first dynode by the collision of an electron with gaseous impurities in the photomultiplier. The event is characterized by correlations in time between single electron pulses and large pulses. A characteristic time for this photomultiplier was 0.4 μsec. In photomultipliers of different design, afterpulses coming 40 nsec later are seen and are due to feedback of light produced at the anode by charge pulses (*4*). Cosmic ray pulses are due to the production of Cherenkov radiation in the photomultiplier window by the fast particles. These ultrashort pulses occur at the rate of about 0.3 counts/sec for this 5 cm diameter photomultiplier and appear to saturate the output at about the 15 photoelectron level for typical gains. The cosmic ray particles also excite fluorescence in the window with a decay

time of the order of 20 to 50 μsec and so generate more correlated noise pulses. The large noise pulses do not have a particularly serious effect on single photon detection since they are each standardized to one count in the discriminator. At low signal rates with an otherwise quiet photomultiplier, the cosmic ray pulses or pulses due to radioactivity in the tube envelope can be serious. At low rates, however, one could use a single channel analyzer to eliminate both small and large noise pulses.

The predominant photomultiplier noise is single electron noise. Its magnitude depends on both the particular photosurface and particular photomultiplier in use. Coates (*21*) studied photomultipliers with bialkali photosurfaces. A typical room temperature noise rate was 200 counts/sec. The single electron noise consisted of two parts: thermal emission from the photocathode and an excess noise apparently generated by field emission. The thermal emission could be eliminated by cooling the photomultiplier to 0°C or below where the excess noise became dominant at about 50 counts/sec. The excess noise shows a nonrandom behavior (approximately $1/f$ in character) and will affect single photon detection (Section II,G,1). It also usually increases greatly with photomultiplier gain and so may become serious if high gains are required. If the application allows, one might use an amplifier to lower the gain operating point of the photomultiplier. Red sensitive photosurfaces show much higher thermal dark noise so that selection and noise reduction become very important for single photon detection. Table III lists typical room temperature noise rates for various photocathodes. Cooling of the photodevice is a popular method of noise reduction. A rough rule of thumb is that the noise rate drops by a factor of ten for each 20°C drop until the excess single electron noise dominates. Such a rapid dependence of noise on temperature requires good temperature control for single photon detection of weak sources. Foord, Jones, Oliver, and Pike (*22*) give a recent review of noise reduction by cooling in a paper concerned with many aspects of photon counting. Cooling does have the disadvantages of condensations and of Cherenkov radiation produced in windows added to prevent condensation. The other noise reduction techniques require that the incoming light signal be collimated to a small spot or narrow beam. Oliver and Pike (*23*) studied a photomultiplier with an effective small photosurface which was also cooled. They obtained a dark noise rate of 0.459 counts/sec at -20°C which was excess noise, random, and ascribed to radioactivity in the tube window. Another method is to eliminate from the multiplier input optics the electrons from all but a small portion of a large photosurface by means of a magnetic or electrostatic lens. Manufacturers are now making these available. A clever use of a magnetic lens was made by Topp *et al.* (*24*) who combined it with a device to enhance the quantum efficiency of their photomultiplier.

Even more serious than dark noise for many applications is noise genera-

ted by the light signal. If noise electrons can produce afterpulses, photoelectrons can do likewise. Coates (*21*) found about one afterpulse for every 100 photoelectron pulses. Foord *et al.* (*22*) investigated signal afterpulsing for a number of photomultipliers and pointed out their effects on both photon counting and correlation experiments (see Section IV,B) and photometry of weak sources. In some photomultipliers, prepulsing has been observed as mentioned by Meiling and Stary (*3*, p. 25). The signal-correlated noise can be studied by either viewing a light source known to cause random emission of photoelectrons in a series of photon counting intervals or viewing it with a multichannel time analyzer as outlined in Section IV,B,3.

2. *Device Noise in Channel Photomultipliers*

The dark noise pulse height distribution of the channel photomultiplier is effectively the same as the single photoelectron distribution when the channel multiplier is operated in the pulse saturation mode. However. the amount of noise is substantially lower compared to a photomultiplier. Wolber (*17*) reports noise counts of from 1 to 10 counts/sec for an S-20 photosurface at room temperature and attributes them to thermionic emission from the photosurface. The low noise rate is due primarily to the small size of the photosurface (1 mm^2). Again collimated light signals are required if a single channel is used. A reduction of 20 in the noise was observed upon cooling to $-20°C$, but no further reduction was observed at lower temperatures. Replacement of the photocathode with a blank disk reduced the room temperature noise rate to 0.01 counts/sec and indicated the cosmic ray contribution. The discrepancy between the cooled rate and the blank rate is probably due to excess noise although the smoothness and continuity of the channels should minimize that source. The conditions for ion noise and time-correlated afterpulses are much more restrictive in the small channels, but they may be present. Afterpulses would cause the same problems in applications as with photomultipliers and should be studied.

3. *Background Noise*

In some applications, single photoelectrons from a light background could obscure the signal photoelectron. Reduction is again the only alternative in the form of spatial filtering, spectral filtering, or time gating. An extreme example of the background limitation is the detection of a single photon against the combined background of bright moon and bright sky as in the Lunar Laser Experiment (see Section III,D,2). A 6 arcsec field of view and a 1 Å wide filter still allowed about 300 kcounts/sec of noise using the 2.7 m diameter McDonald observatory telescope. The final reduction

technique required the setting of a microsecond time gate about the expected time of arrival of the lunar return by electronic means. A number of repeated rangings were, of course, necessary to be certain of a signal return. It is also of interest to note here that the photomultiplier used had to be operated at very high gains and so was subject to excess noise. The ERMA photosurface which was used exhibited a noise rate of 30 kcounts/sec at room temperature and several kcounts per second when cooled to about 0°C.

D. Practical Photodevice Techniques and Photon Detection Performance Tests

It is important to be able to measure the SER amplitude distributions of both single electron signals and noise in order to evaluate the single photon detection capabilities of a particular photodevice. These tests also enable one to be sure that correct photodevice techniques are being employed. Poor practices can greatly increase photodevice noise and may lead to destruction of either the photosurface or the device. Table II gives a checklist of good

TABLE II

CHECKLIST OF GOOD PHOTON COUNTING PRACTICE WITH PHOTOMULTIPLIERS

Housing design	Practice
a. Optical isolation	a. Test housing before inserting tube
b. Electrostatic, magnetostatic, and rfi shields	b. Ground photocathode (if at all possible)
c. Insulating material choice and placement	c. Never expose tube to strong light
d. Stable, high frequency electrical components	d. Keep clean of cloth fibers, moisture, etc.
e. Dissipation of heat from divider resistors	e. Use as low a gain as possible
f. Stable cooling method free of electrical noise	f. Allow device noise to stabilize
g. Cooling scheme free of condensation	g. Use stable, low noise high voltage supply
h. Tapered divider and charge-storage capacitors	h. Good high frequency wiring technique

practices; a number of which seem always to be ignored in homemade and commercial photodevice units. Recent discussions of performance tests and good photodevice techniques have been given by Morton (*7*), Zatzick (*19*), and RCA staff (*4*). If afterpulsing can seriously affect a particular single photon detection experiment, additional tests for time correlations should be made as discussed in Section IV,B,3.

Morton (7) gives a concise summary of tests for single photon counting performance of photodevices based on Fig. 1. First in importance is the determination of the location and shape of the single photoelectron peak. An approximate location of this peak can be found by setting the threshold of the integral discriminator at its lowest value and by examining the dark noise as a function of tube voltage. The presence of a peak in the single electron pulse height distribution will be recognized by the occurrence of a plateau in this integral voltage curve. If the noise rate on this plateau is sufficiently low, one can study the single photoelectron peak by illuminating the photosurface with a steady, weak light source which yields a count rate about ten times the noise rate and examining the count rate as a function of discriminator level. The result should be an integral curve similar to that in Fig. 4. To express the abscissa in terms of equivalent electrons, one sketches in the rectangle shown with height equal to the total number of electrons observed and whose area is the area under the integral curve. The intercept of this rectangle on the abscissa gives the height of one photoelectron. The slope of the integral curve gives the SER amplitude distribution. The use of a multichannel pulse height analyzer obtains the amplitude distribution directly and greatly reduces the time necessary for these tests. However, the tests should be done as close as possible to the operating conditions of a particular experiment which may preclude the use of an analyzer. It is sometimes necessary to subtract the integral curve of the device noise in order to interpret the single photoelectron distribution. In any case, a careful study of the device noise amplitude spectrum (e.g. Fig. 5) is necessary in order to set a lower (and upper if used) discriminator level to optimize noise discrimination with a known loss of single photoelectron pulses. If cooling is necessary, the tests should be done under these conditions. SER amplitude distributions can be examined in the presence of high device noise by using the time-gating method discussed in Section III,C,1. Finally, one should investigate the statistics of the counting process for device noise by repeated counting since this is one of the factors limiting detection measurements of weak sources. Deviations of the signal counting statistics from random behavior is discussed in Section IV,B.

E. Quantum Efficiency of Photosurfaces

1. Introduction

The photosurface of the photodevice converts incident signal photons into photoelectrons which enter the multiplier to be detected. The efficiency of this conversion, η, at the wavelength of interest, λ_1, is therefore very important for single photon detection. It is called the photosurface quantum efficiency and is usually quite a lot smaller than 100%. If one were simply

trying to detect a signal photon in a gated interval in the absence of noise, it is obvious that the probability of detection increases directly with the quantum efficiency at the wavelength of interest. If a background photon noise rate, N_B, and a device noise rate, N_d, are present, the probability of detection depends on the accumulated photoelectron signal, ηn_p, becoming larger than noise fluctuations in the expected interval after repeated trials. Assuming that both noise and signal fluctuations can be described by Poisson statistics, one can obtain the signal to noise ratio, S/N, as

$$S/N = \eta n_p/(\eta n_p + \eta N_B T + N_d T)^{1/2}, \tag{9}$$

where it has been assumed that the noise has been measured in an equal time interval where the signal was not present and T is the total time of observing both intervals. A similar result is obtained for photometry of weak sources in Section II,G,1. If device noise dominates and the photoelectron signal is written in the form of a rate, (9) reduces to the expression for the figure of merit of a photodevice for photon counting given by Morton (*7*). In this case, it is possible that one would select a photodevice with a lower noise to maximize this figure of merit rather than a higher η. In all other cases, the choice is the highest quantum efficiency.

A history and description of most available photosurfaces is given by Sommer (*25*). A review to mid-1970 is given by Bell and Spicer (*26*). Table III is compiled from these sources plus RCA Staff (*4*) and includes the properties of some of the older photocathodes as well as those of the new photosurfaces

TABLE III

TYPES AND CHARACTERISTICS OF VARIOUS PHOTOSURFACES[a]

Cathode type	Stoichiometry	Wavelength of peak response (Å)	Peak quantum efficiency (%)	Wavelength at 1% peak quantum efficiency (Å)	Dark noise rate at 20°C (e/cm²/sec)
S-1[b]	Ag–O–Cs	8000	0.5	12,000	5×10^6
S-11	Cs_3Sb–O	4000	15	6300	100
S-20	$Na_2KSb(Cs)$	4100	19	8300	400
Bialkali	K_2CsSb	3800	30	6600	30
ERMA	Na–K–Sb–Cs	5600	10	9300	10^3
GaAs	GaAs(Cs)	3400	12	9000	10^4
GaAsP	$GaAs_{1-x}P_x$	3300	17	7400	10^4
GaInAs	InGaAs–CsO	4000	22	10,500	—

[a] Dark noise rates from Zatzick (*19*). Other data from Sommer (*25*) and RCA staff (*4*).
[b] Above 4000 Å.

that have been developed for use in the near infrared. The ultraviolet response of conventional photosurfaces is generally limited by the device window. New materials are sought for this region primarily for lack of sensitivity at longer wavelengths. Table III lists peak quantum efficiency, a measure of the span of the spectral response, and dark noise rates. Spectral response curves can be found in the references. The quantum efficiency at a given wavelength is related to the commonly used radiant spectral sensitivity, σ, in mA/W by

$$\eta = 1239.5\,\sigma/\lambda_1, \tag{10}$$

where λ_1 is in Ångström units.

2. *The Photoemission Process*

A concise description of the photoemission process will be useful at this point for a number of reasons. It aids in the understanding of the improved yields of photoemission and secondary emission of the new materials, their effects on device time resolution (see Section III,A), and quantum efficiency enhancement in the older photosurfaces. Even prior to the development of the new materials, a basic description of the efficient conventional photosurface was achieved on the basis that they were semiconductors (*25*). Figure 6 shows an energy model for a semiconductor photoemitter which includes the space dimension normal to the surface. The valence band is the highest filled energy band for electrons. Immediately above the valence band is an energy gap of width E_G for which no energy states exist for electrons. Above this forbidden band, there is a band of permitted energy states (i.e. the conduction band) which at ordinary temperatures contains very few electrons.

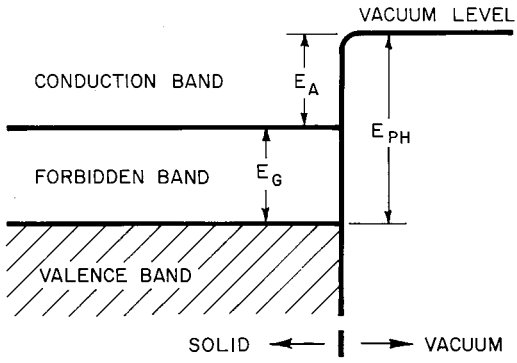

FIG. 6. Energy band model for a semiconductor photoemitter. Distance from surface also shown. Threshold for photoemission is $E_{PH} = E_A + E_G$. E_A is electron affinity energy.

An electron at the bottom of the conduction sees a potential barrier for emission to the vacuum represented by E_A which is called the electron affinity energy. Photoemission from the semiconductor for a photon of energy E_{PH} may then be viewed as a three-step process; absorption of the photon by the material and excitation of an electron from the valence band to the conduction band, movement of the excited electron to the vacuum interface, and escape of the electron over the potential barrier into the vacuum. Therefore, the minimum photon energy necessary to produce a photoelectron is the sum of E_G and E_A. This minimum sets the limit of red response. For example, the S-20 photosurface has an E_G of 1.00 eV and an E_A of 0.55 eV. The absence of thermal electrons in the conduction band and the typical E_A which are much smaller than impact ionization thresholds mean that the electron excited to the conduction band can escape from moderately large depths compared to a metal; being limited only by energy loss through electron–phonon interactions. This large escape depth leads to high quantum efficiencies as long as the wavelength-dependent absorption coefficient is high enough. Typical escape depths for conventional photosurfaces are about 200 Å compared to 10 Å in metals.

The addition of the concept of negative electron affinity to the above description started a search for suitable photoemitters among the more familiar semiconductors. Negative electron affinity means that the energy bands near the surface of the semiconductor are bent in such a way that the bottom of the conduction band deeper inside the surface lies above the vacuum energy as shown in Fig. 7. This bending can be accomplished by the adsorption of electropositive metal atoms on the surface of a sufficiently *p*-type bulk semiconductor (such that its Fermi energy is at or near the edge of the valence band). The depth of the bent band region should be as small as possible. The great advantage of materials with negative electron affinity is

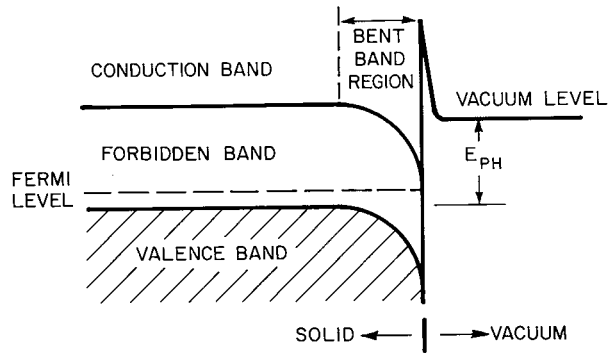

FIG. 7. Energy band model of a semiconductor photoemitter with negative electron affinity. Distance from surface also shown.

that the majority of electrons excited to the conduction band and traveling slowly toward the surface can be emitted even though they lose energy in phonon collisions. Even those electrons excited deep within the material (up to 10,000 Å) have a reasonable probability of being emitted as photoelectrons into the vacuum. Consequently, the photosurface quantum efficiency is greatly enhanced, especially near the threshold. The limit of red response is approximately equal to the semiconductor band gap (e.g. 1.4 eV in GaAs–Cs). Scheer and van Laar (*27*) reported the first photosurface (GaAs–Cs) built on this concept in 1965. The practical utilization of these concepts had to await the development of high quality semiconductors with appropriate band gaps and doping levels and with good minority carrier transport properties. Most promising for practical and commercial applications are the III–V compounds. The incorporation of the new photoemissive materials into photomultipliers is proceeding rapidly. Reports on the performance of these new photomultipliers have not yet reached the general literature although some numbers are available in Table III. The energy distribution of photoelectrons may be narrowed as for secondary electron emission, at least for shorter wavelengths. A greater effect on time resolution could come from the long electron diffusion times (e.g. 100 psec) associated with the greater escape depths. This effect does not at present limit the time response of photodevices, but may if materials with greater escape depths are used to obtain higher quantum efficiencies.

Cooling of a photosurface to reduce dark noise can affect the quantum efficiency of the photosurface. Boileau and Miller (*28*) report that a lowering of the temperature usually increases the short wavelength efficiency, but decreases the long wavelength sensitivity. The increase is minor while the decrease can be as much as 2% per °C near the photosurface threshold. If one is working in the long wavelength region and is cooling the photosurface, one should measure the quantum efficiency at the operating temperature. In any case, the temperature of the photosurface should be kept constant in in order to have a stable efficiency photomultiplier. It is best to assume that a given photosurface has a large temperature coefficient in the far red until proven otherwise.

3. *Measurement of Photocathode Quantum Efficiency*

It is often necessary to measure the quantum efficiency of a photosurface in order to check its uniformity over the surface, to check its relative spectral behavior, to examine its temperature dependence at a given wavelength, or to measure an absolute value at a certain wavelength. These and other basic tests of a photodevice are described in the IRE Standards (*29*). The absolute measurement is difficult to carry out accurately. Relative measurements can

be made more easily (*30*). The photodevice is connected as a diode if possible with all other electrodes at a potential of several hundred volts. The cathode current is then measured for a constant amount of light at the wavelength of interest as the conditions are varied. If the wavelength is varied, a thermopile or some other secondary standard is needed to monitor the light intensity. If a rough measure of the quantum efficiency is sufficient (i.e. to about 10%) and the secondary standard is stable and previously calibrated, the quantum efficiency in electrons per photon can be calculated.

4. Quantum Efficiency Enhancement

Quantum efficiency enhancement really consists of the reduction or elimination of losses which occur at the photocathode (*25*). Before the new materials, all photocathodes were deposited as thin layers on opaque or transparent substrates. Aside from the obvious reflection losses at the photocathode interfaces, there are two other types of losses: transmitted light and light absorbed beyond the escape depth. These losses are wavelength dependent because the absorption coefficient of the photosurface material usually varies with wavelength. One method of enhancement increases the light path (and absorption) without going beyond the escape depth by depositing the photosurface on a reflecting substrate. The enhancement is usually greatest in the red where the absorption coefficient is lowest. A further improvement is to make the photosurface part of a reflection interference filter which, however, limits the range of useful wavelengths. These techniques are not particularly useful with the new materials which are already near optimum absorption and escape depth and which are small bulk semiconductor crystals mounted as an integral part of the multiplier. In addition, most older photomultipliers were designed for use with diffuse light sources and so required large, transmission-type photosurfaces. These transmission-type photocathodes have thicknesses chosen to maximize their response toward the blue. Much of any incident red light is transmitted through the photosurface resulting in low quantum efficiencies. Thicker photosurfaces would help, but would soon be limited by the escape depth problem in addition to lowering the blue response. These photocathodes can have their red response enhanced by external optical techniques that prolong the light path inside the photocathode without causing it to move too far from the surface. Gunter, Grant, and Shaw (*31*) give a good review of these techniques and practical results with several tube types. Enhancements of about two were obtained in the blue and up to six in the red and near-infrared. Optical enhancement requires narrow, collimated beams as do the photomultipliers with the new photosurfaces. Finally, Crowe and Gumnick (*32*) report enhancements with conventional photosurfaces as a result of the application of external electric

fields. This enhancement may be due to a lowering of the vacuum potential barrier shown in Fig. 6. Enhancements of 3 to 6 were observed near 9000 Å. The same enhancement technique may be applicable to the new photoemitting materials.

F. Total Quantum Counting Efficiency

The photoelectrons released from the photosurface of a photodevice may not all be detected as counts at the discriminator for a variety of reasons. The total quantum counting efficiency of the device will therefore show a discrepancy compared to the photosurface quantum efficiency. The discrepancy may occur due to inefficient collection of photoelectrons at the first multiplier surface, losses in the multiplication process, or rejection of the smaller pulses of the SER amplitude distribution by the discriminator. Pietri (*33*) measured the collection efficiency of an early high gain, focused photomultiplier to be 80% at 4200 Å for a 2 cm^2 spot at the center of its photosurface. He was able to redesign the input optics in a later tube to raise the collection efficiency to near 100%. The collection efficiency was found to decrease with an increase in the area of the photosurface used and to increase as the wavelength of the incident light was increased. The collection efficiency of most photodevices and its behavior with wavelength and position can be predicted by computer simulation of electron trajectories in the photocathode–first dynode region (*4*). Focused photomultipliers are designed to give collection efficiencies from 85% to 98% depending on the size of the photosurface used. Other geometry photodevices may have lower collection efficiencies. Wolber (*17*) quotes a lower bound of from 70 to 90% for a channel multiplier. Loss of counts in the multiplier would not be expected to affect discrete dynode multipliers, as discussed in Section II,B,3. However, this loss might be expected to be more serious in devices which have low initial multiplication factors.

The possible source of discrepancy most easily studied is the rejection of small pulses by the discriminator. Although it can be taken into account in experiments by knowing the SER amplitude distribution and the setting of the integral discriminator, observing times still depend on the detected signal rate. The high gain, first dynode photomultiplier discussed in Section II,B,3 should enable one to work on a counting plateau where a very large percentage of the single photoelectrons are detected and thereby to achieve a counting efficiency very close to the photocathode quantum efficiency. Lakes and Poultney (*30*) have made a direct measurement of these two quantities for this photomultiplier and find about a 25% discrepancy even though an excellent counting plateau was observed. Birenbaum and Scarl (*34*) later found a 40% discrepancy, but with a plateau of significant slope at their operating gain. They attributed the discrepancy to an unexpected number of photoelectron

pulses much smaller than the well-behaved single photoelectron peak. Figure 5 gives an indication of the deviation at small pulse heights. Coates (*35*) has studied such a deviation of the SER amplitude distribution from the predictions (Section II,B,3) for this particular photomultiplier and was forced to propose an edge effect after considering many other causes. The edge effect consists of a loss of electrons from a charge packet due to striking either the edge of a dynode or a macroscopic inhomogeneity on a dynode. Again this photomultiplier allows a very detailed investigation of its own behavior. It is not now clear whether this otherwise excellent photomultiplier has a unique problem or whether the poorer SER ampitude distributions of other photomultipliers manage to mask the effect. In any case, workers should be aware of the possibility that the total quantum counting efficiency of a photodevice may be lower than the photosurface quantum efficiency. The discrepancy can cause longer observing times, in the least, and unexpected systematic errors in photometric applications.

G. Typical Photon Detection Experiments

1. Introduction

There are a wide range of photometry and spectrophotometry experiments that require the measurement of a weak light intensity. The weak intensity may be due to a weak source, scattering with small cross sections, or many spectral channels viewing a stronger source. With the assumption that the photodevice has been selected for optimum quantum counting efficiency, η_0, one can define weak light intensity as about 100 counts/sec or less. The photodevice is operated as shown in Fig. 1 for single photon detection which is also called photon counting. The anode charge pulse is detected at the discriminator, standardized, and recorded by a digital counter. If there are no correlated afterpulses and if the device and background noise rates are much smaller than the signal rate, the fractional precision of a measurement (i.e. the inverse of the signal to noise ratio) is given by

$$(S/N)^{-1} = 1/(\eta_0 N_P T/2)^{1/2}, \tag{11}$$

where N_P is the signal photon rate and $T/2$ is the measurement period. The signal counts are Poisson distributed in time or shot noise limited, at least for coherent and broadband light. Alternate detection and recording methods do exist in which analog recording (i.e. a rate meter or current meter) can be used on either standardized or nonstandardized photodevice output pulses. Jones, Oliver, and Pike (*36*) show theoretically and experimentally that photon counting yields the best precision as given by (11) in a given observation

period. A rate meter (i.e. analog recording) viewing standardized counts is shown to yield a fractional precision lower by $\sqrt{2}$ and therefore requires twice the measurement period to obtain the same precision. This result can easily be obtained from Campbell's theorem for the situation in which one observes for a period four times the integration time of the rate meter. An additional lowering of the fractional precision of a measurement in a given period enters if nonstandardized counts are recorded. For an SER amplitude distribution which fits the theory outlined in Section II,B, the fractional precision is lowered by the square root of $(1 + \varepsilon_A{}^2) = 1 + (\Delta/2.35)^2$ where ε_A and Δ are defined in Section II,B. This factor becomes $\sqrt{2}$ for a photodevice without a peak. The particular choice of detection method depends on the signal rate. Photon counting is superior at very low signals rates, but does have a high signal limit. Near or above this limit one must switch to analog recording of nonstandardized pulses. At signal rates in between these two limits, the method is probably determined by past practice and simplicity of record keeping. One advantage of photon counting is that it allows one to make a detailed study of the photodevice being used. Further advantages of photon counting are discussed below for a number of typical experiments. The presence of η_0 in (11) should also be noted.

Assume now that the photodevice in use is being operated under optimum conditions as discussed previously so that a counting plateau exists and the dark noise and background rates have been reduced to about 1 count/sec. As the signal rate approaches 1 count/sec, the observation period needed to obtain a certain precision will increase over that predicted by (11). This increase can be obtained from

$$(S/N)^{-1} = (\eta_0 N_P + 2\eta_0 N_B + 2N_d)^{1/2}/\eta_0 N_P (T/2)^{1/2}, \tag{12}$$

where N_P, N_B, and N_d are the signal photon, background noise photon, and dark noise rates, respectively. The signal has been separated from the noise by effectively modulating the source with a square wave of period T and the noise is also assumed to be Poisson distributed in time. Again, any of the alternate detection methods can be used with the fractional precision (12) lowered as discussed above for the shot noise limited expression (11). It should be pointed out that synchronous analog detection has additional noise discrimination advantages over a straight current measurement (*37*), due to low frequency circuit noise not considered above. Synchronous digital detection has no such advantage over photon counting. Its advantage over all other methods beyond those already discussed is its low drift operation with time which allows very long observation periods (of the order of hours). Synchronous photon counting was first reported by Arecchi, Gatti, and Sona (*38*) and somewhat later by Oliver and Pike (*23*). A more sophisticated

version with provisions for readouts of signal and noise as well as the difference and sum for assignment of statistical uncertainty was recently reported by Zatzick (*19*). Their results are consistent with the determination of a signal of 0.1 count/sec with a precision of 10% ($S/N = 10$) in the presence of 1 count/sec Poisson-distributed noise using a counting period of one hour. Predictions for other signal and noise rates can be obtained from (12). Again note the advantage of the highest possible total counting efficiency.

The high signal rate limit of photon counting is determined by the response times of photodevice, amplifier, discriminator, or digital counter. Usually, the dead time of either the discriminator or counter sets the limit. The recent version of the synchronous digital photon counter has a limit of 85 MHz yielding a practical intensity range of about 10^8. However, this upper limit may have to be lowered considerably if it corresponds to an anode current limitation of a photodevice or if afterpulses are present. One way to eliminate the effect of afterpulses is to gate the detector off until after the characteristic time of afterpulsing (e.g. 10 μsec). Rather than switch to other detection methods from photon counting, one has the final alternative of attenuating the incoming signal with calibrated filters.

The deviation of the signal and noise rates from a Poisson behavior due to the photodevice will lower the precision of a measurement below (12) in a fixed observation time. The same is true for deviations due to fluctuations in the light intensity. However, here a study of the deviations in the counting statistics would reveal information as to the nature of the light source, or the scattering medium as discussed in Section IV,B. The deviations due to the photodevice which are discussed in Section II,C,1 can also dictate the choice of detection method. For example, the residual noise component due to cosmic rays occurs at a very low rate, but yields very large pulses. If measurements are made on weak sources using nonstandardized pulses, the large pulses can cause serious systematic errors (*39*). In addition, afterpulsing can only be eliminated in the photon counting mode. The most serious deviation due to photodevice from a diagnostic viewpoint would be the presence of single electron afterpulses several microseconds after every dark or signal count. Neither pulse height spectra nor a cursory counting statistics study would uncover it and a systematic error in source intensity would result. Probably only a study of the arrival times of each count by the methods of Section III,C would catch it.

2. *Laboratory Photometry and Spectrophotometry*

Weak source photometry in the laboratory includes measurements of the angular and polarization dependence of light scattered from either single particles (*40*) or from the cooperative effects of many particles (*41*). These

measurements can be used to study the sizes and other properties of individual particles and to study the correlation lengths for cooperative particle or density fluctuation effects. Low light level spectrophotometry includes the measurement to medium or high resolution of the spectra of any weak source or of any scattered light. The threefold advance of recent years in laser light sources, high resolution (and high background rejection) spectrometers, and photon counting has had a profound effect on the study of matter by light scattering. Smith (*42*) gives a brief review of the many different collective motions in matter now being studied by combinations of these techniques. Accessible with tandem monochromators are weak Raman-shifted frequencies (10^{12} to 10^{13} Hz) of light scattered from molecules and from various optical modes of excitation in matter as well as smaller frequency shifts previously obscured by conventional source linewidths. Accessible with high resolution, scanning Fabry-Perot interferometers are weak Brillouin-shifted frequencies (10^{9} to 10^{11} Hz). Chu (*43*) briefly reviews recent Raman and Brillouin scattering studies, discusses Rayleigh scattering studies using optical mixing spectroscopy, and recommends the photon counting statistics discussed in Section IV,B as an alternate to that new spectroscopy.

Single photon detection is only used in these types of experiments for the weakest intensities. Reynolds (*44*) reviews an interesting series of photon detection experiments with interferometers and slit systems which demonstrate that the interference patterns are obtained as expected with very weak sources. Both photomultipliers and image tubes were used. Arecchi *et al.* (*38*) used their synchronous photon counter to measure the angular distribution of Raman scattered light from the 992 cm^{-1} vibrational frequency of benzene in a direction parallel to the polarization plane. A He–Ne laser at 6328 Å was used as the excitation source. Signals as low as 10 counts/sec were measured to 10% precision with observation times of 1 min in the presence of noise of 500 counts/sec from the uncooled RCA 7265. An example of photon detection as applied to Brillouin scattering in gases is given by Greytak and Benedek (*45*). They use an ITT FW130 with 3 dark counts/sec and state that signal shot noise limited the precision. Their peak signal rate was 300 counts/sec. Lineshifts of about 10^{8} Hz and linewidths of about 3×10^{7} Hz (nearly equal to instrumental width) were measured. Background scattered light had to be subtracted. Barrett and Adams (*46*) give an excellent description of the many related techniques used to improve signal to noise ratios in a study of Raman scattering from rotation–vibration lines in ultrasmall gas samples. These techniques include sample illumination, polarization discrimination against Rayleigh-scattered light, optimum collection of scattered light, and single photon detection. An EMI 6256S photomultiplier was used at a peak signal rate of about 10 counts/sec resulting in a total of a few hundred pulses for a typical rotational line in the vibration band. The dark count was

46 counts/sec at room temperature and one count every 5 sec when cooled to about −40°C. A rate meter-type recorder was also provided for viewing the standardized pulses. The monochromator was scanned at as low a rate as 1.8 cm^{-1}/min for a total scan time of three hours in the case of the rotation–vibration (1–0) band in nitrogen. An integration time of 10 sec was used for counting. The magnitude of the background was not mentioned. Mooradian (*47*) considers the elimination of unwanted excitation radiation as one of the most difficult experimental problems of laser light scattering spectroscopy and refers to several electronic and optical subtraction techniques that have been successfully employed. Most of these techniques are coupled with synchronous detection. The unwanted radiation becomes most troublesome in the spectral region near the laser line itself and even several monochromators in tandem cannot reject it sufficiently. The resolution, scan rates, and integration times of weak source spectroscopy will depend on the aims of the particular experiment as well as the signal to noise ratio. The decision to move to single photon detection and most likely to synchronous digital detection probably requires the recording and processing of the data in digital form. Commercial manufacturers of spectrometer systems now offer the whole range of detection and recording methods mentioned in Section II,G,1.

3. Photometry and Spectrophotometry in Astronomy

Interest in the detection and measurement of faint astronomical sources has always constituted an impetus to single photon detection. An early review of this work can be found in the articles by Baum, Johnson, and Lallemand in the volume edited by Hiltner (*48*). Photometry and spectrophotometry in astronomy differ from those in the laboratory in that other natural phenomena affect the measurements and other workers are waiting to use the costly facilities. The natural phenomena include atmospheric "seeing," scintillation, and extinction. In addition, the night sky background may fluctuate due to physical processes. Background can be subtracted by means of a two-channel photometer with one detector viewing a nearby patch of dark sky or by means of a one-channel photometer synchronously switched from star to dark sky in conjunction with the synchronous digital detection mentioned in Section II,G,1. The switching can be done either in the telescope optics or in a photomultiplier designed for magnetic deflection of a viewing spot on the photosurface. Tull (*49*) describes a photon counting system for high resolution spectrophotometry and includes a discussion of the atmospheric and other noise limitations. Zatzick (*19*) briefly describes a 32-channel photon counting spectrometer attached to the Mt. Palomar 5 m telescope. Each photomultiplier views a different region of the spectrum and is interfaced with a computer for data recording, background subtraction, and

limited data analysis. The typical light flux may be about 1 or 2 photons/sec so that spectral information from stars of 22nd magnitude can be obtained. The need to perform calibration measurements on bright stellar objects with known properties requires the additional capability of fast counting devices and circuitry. Dennison (*50*) has recently described the philosophy and practice of electronic optical astronomy and includes therein new developments with single photon detection in astronomy. Rather than use 32 or 80 photomultipliers one would like to use a single image tube with an electronic readout of the image of a weak source or spectrum. At present, the image intensifier is used as the front end of such an image tube and its single electron detection properties determine those of the whole device. Methods of evaluating the single photon detection capabilities of image intensifier tubes have been pioneered by Reynolds (*51*) and have many similarities to the evaluation of photomultipliers.

III. Fast Timing with Single Photons

Fast timing with single photons means that the timing system consisting of a photodevice, timing circuits, and timing methods is capable of measuring the interval between single photon events to nanosecond or better accuracy. The capability of counting photons at high rates is closely related; especially if the interval between events being timed is very small. In addition to this timing capability, the fast system must possess all the single photon properties outlined in Section II. In special cases such as background noise limited detection or a surplus of signal photons, this last requirement can be relaxed by allowing a high device noise or by allowing a poor counting efficiency respectively as noted in Section III,D.

A. Photodevice Timing Capabilities and Limitations

Photomultipliers with discrete linear dynodes and electrostatic focusing (see Fig. 3) have long held the lead in precision timing of intervals between single photon events or between a time marker and a photon event. Many of the properties which placed them foremost in efficient single photon detection also aid in the attainment of this fast timing and counting. Efficient photon detection is not, however, a sufficient condition for fast timing. A review of the timing capabilities and limitations of this particular type of photomultiplier will establish a framework for the comparison of present devices and for the contemplation of new devices. Several of these new devices can be expected to yield an order of magnitude improvement over present photomultipliers.

Most devices operating on the principle of external photoemision possess three basic elements; a photosurface with electron optics which directs the photoelectron into the electron multiplier, the electron multiplier which amplifies the single electron by secondary emission, and the anode which collects the charge packet to provide an external signal (see Fig. 1). The time of travel from the photosurface to the external output lead is called the electron transit time, h, of the device. It can be measured using a short light signal of single or multiple photon intensity which has a synchronous electrical pulse. The arrival time of the resultant charge pulse at the external output must be defined with respect to a characteristic of the pulse such as its centroid or a point part way up its leading edge. This arrival time will fluctuate from one measurement to another, especially for single photon signals. This fluctuation in device transit time will limit the timing precision for single photon events and will be assumed to consist of transit time fluctuations or spreads between photosurface and multiplier, ε_{KM}, in the multiplier, ε_{MS}, and between multiplier and anode, ε_{MA}. These spreads originate both in the geometry of the device and in the distribution of initial velocities of photo and secondary electron emission. For example, the geometry may be such that all possible electron paths between two device elements are not isochronous for even the electrons emitted at rest. The individual spreads will be expressed as standard deviations and added as such with suitable weighting factors. Values for the individual transit time spreads and their dependence on photodevice design are discussed below. It might be expected that initial stages of a photodevice contribute with the greatest weight to the total transit time fluctuation. In the later stages, the growing number of electrons in a charge pulse provides many samples of the transit time of a stage and should reduce the transit time fluctuation of that stage in the manner of the standard error of a mean (i.e. the transit time variance of that stage divided by the number of electrons sampling the paths). With the assumptions that all transit time spreads after ε_{KM} are equal ε_{SS}, that all stage multiplications are equal (i.e. g), and that multiplication fluctuations do not have a significant effect on the spread weighting factors, one can express the total transit time fluctuation for a photomultiplier as

$$\varepsilon_{PH}^2 = \varepsilon_{KM}^2 + \varepsilon_{SS}^2/(g-1), \tag{13}$$

Gatti and Svelto (*52*). The first stage or dynode often has a larger gain g_1 as well as a larger ε_{SS} as discussed below. In this case, the single photon transit fluctuation of the photomultiplier would be approximated by

$$\varepsilon_{PH}^2 = \varepsilon_{KM}^2 + \varepsilon_{S1S2}^2/g_1 + \varepsilon_{SS}^2/(g-1)g_1. \tag{14}$$

Thus the high multiplication factors that yield good SER amplitude distributions also yield better time resolution. Time resolution, R, is related to the

transit time fluctuation by 2.35 ε_{PH} and is the experimentally observed quantity (see Section III,C). Single photon time resolutions of as low as 320 psec have been measured for a particularly fast photomultiplier by Birk, Kerns, and Tusting (*53*).

If the charge pulse collected at the anode is neither saturated nor ringing, the anode pulse width can also be estimated from the transit time spreads, but with different weighting factors. The anode pulse for a single photon is called the single electron time response and can often be approximated by (4). Its full width at half-maximum, P, is given by

$$P = 2.35\lambda = 2.35(\varepsilon_M{}^2 + \varepsilon_{MA}^2)^{1/2} = 2.35[n\varepsilon_{SS}^2 + \varepsilon_{MA}^2]^{1/2}, \tag{15}$$

where n is the number of identical multiplications and λ is the width of the single electron response in terms of a standard deviation. The front stages no longer dominate so that a device with a very narrow anode pulse need not have exceptional time resolution. Gatti and Svelto (*52*) also show that the variance of λ is much smaller than the total transit time fluctuation ε_{PH} for the usual case of a number of multiplications in a multiplier at moderate gains. This conclusion further supports the use of a standard shape for the single electron time response of a photomultiplier. Birk and co-workers (*53*) find a single electron response of roughly Gaussian shape with a full width P of 0.8 nsec for the fast photomultiplier. This response is best measured in real time with single (or multiple) photon light pulses of sufficiently short duration. This time response sets the limit to the counting rate at high levels and, through a Fourier transform, to the frequency response of the photodevice. Great care is necessary in the design of the anode to minimize ringing and saturation which will cause an additional decrease in counting rate and frequency response. Pietri (*54*) outlines a number of these precautions as well as raising the specter of a transit time fluctuation related to saturation of larger pulses. RCA staff (*4*, pp. 24, 107) give some advice about preserving the device time response at the anode and at the external connection. Saturation and ringing tend to affect the falling portion of the time response and usually do not limit timing resolution. When these are present, connection with (15) can still be made for a study of ε_{SS} by using the rise time of the pulse.

A general theory of the statistical time behavior of a photodevice could be constructed as summarized by Donati *et al.* (*12*). The probability density functions of transit times in each element of the photodevice would have to be calculated or measured and then convoluted together. To calculate the probability density functions, one would need to know photodevice geometry, element potentials, element multiplication factors g, and the distribution of photoelectrons and secondary electrons in energy and angle of emission. This general theory would also necessarily include the amplitude fluctuations

previously treated. However, there may be a correlation between the probability density functions of successive stages which would render even a numerical convolution inaccurate. The analysis of the electron trajectories and transit times in a device with given geometries and potentials is in practice done numerically by computer simulation [Krall and Persyk (*55a*)]. The assumption made above of the Gaussian behavior of individual spreads and the use of (13), (14), and (15) is an attempt to estimate and compare the timing capabilities of various photodevices without doing the detailed calculations.

1. Photomultipliers

a. Conventional fast photomultipliers. Conventional fast photomultiplier here means the type in Fig. 3 with transmission-type photocathode, electrostatic focusing, and linear, discrete dynode multiplier. Typical single photoelectron transit time fluctuations ε_{PH} are about 0.5 nsec. Pietri (*54*) and Pietri and Nussli (*5*) give a particularly clear account of the design, characteristics, and improvement of a photomultiplier of this type. The large contributor to the ε_{PH} of this and many other types of photodevices is the transit time spread ε_{KS1} in the photocathode–first dynode transit time. This spread shows up of course only after repeated measurements with single photons and after allowance for later dynode compensation. In a photomultiplier, the ε_{KS1} depends on the geometry, electric fields, and the process of photoemission in the KS1 region. The electrode geometry is usually adjusted so as to equalize the flight times to the first dynode of photoelectrons emitted at rest anywhere on the photocathode. In addition, the photocathode is curved, fields are made uniform in its vicinity, and some compensation is introduced in later dynodes. Any remaining difference for the larger photocathodes is quoted as a transit time difference across the photocathode (e.g. 0.8 nsec). Here it is assumed that only the central portion of the photocathode is used so that the transit time difference is zero. The central photoelectrons can, however, leave the photocathode with different velocities which depend on the process of photoemission as well as the wavelength of the incident light. The transverse velocity component (perpendicular to the mean path of the photoelectron) on average spreads out the target spot on the first dynode. The focusing fields must be configured so as to keep this spot smaller in size than the active part of the dynode for every point on the photocathode in order to achieve good collection efficiency. The transverse velocity spread need not cause a transit time spread except for the need to leave the axial symmetry of the KS1 region and enter the planar symmetry of the multiplier. This change in symmetry means that the first dynode intercepts the electron paths at about an angle of 45° (Fig. 3). The deviation of the next two dynodes from

the linear multiplier geometry is introduced to compensate transit time differences due to transverse velocity spread. This compensation will be assumed sufficient to leave the spread in normal emission velocities as the prime contributor to ε_{KS1}. Assuming the electric field between K and S1 uniform and due to a potential φ over the distances s_1 and with the energy W_n corresponding to the normal component of initial velocity small compared to $e\varphi$, one can esimate the transit time spread by

$$dt_1/t_1 = -(W_n/e\varphi)^{1/2}. \tag{16}$$

The KS1 transit time t_1 is given by

$$t_1 = s_1(3 \times 10^{-8})/\varphi^{1/2}, \tag{17}$$

where s_1 is in cm and φ in V. Large photocathode photomultipliers usually have s_1 equal to or larger than their diameters to aid in flight time equalization and collection efficiency maximization. Typical values of s_1, φ, t_1, W_n might be 7 cm, 300 V, 12 nsec, and 0.3 eV. The ε_{KS1} is then about 3.5% of the transit time or 0.42 nsec. An increase in φ would decrease the ε_{KS1} in direct proportion, but the increase is finally limited by either photomultiplier construction or the need to be near the peak of the secondary emission curve.

The transit time fluctuation in the multiplier also depends on the geometry, electric fields, and the process of electron emission. The linear cascade of opaque dynodes in Fig. 3 is used for good time response as well as minimizing ion and light feedback noise and providing a good SER amplitude distribution. It quickly becomes a regular array after the coupling region where the dynodes are shaped and positioned to compensate transit time differences. Additional focusing fields are provided near each dynode so that the cross section of the electron cloud becomes narrower and narrower as it travels down the multiplier. If it is assumed as above that the geometrical problem has been solved, the secondary emission velocities again determine the transit time fluctuations of each stage of the multiplier. These velocities correspond to energies W_n about ten times greater than those of photoelectrons for conventional materials. An estimate for ε_{SS} can be obtained from (16) and (17) slightly modified assuming that only the velocity spread along the path is important. Typical parameters are $s_S = 2$ cm, $\varphi = 135$ V, and $W_{Sn} = 3$ eV. The modifications consist of a substitution of 2φ for φ in (16) and a substitution of $s_S/2$ for s_1 in (17). These modifications enter because of the effect of the $n+2$ dynode on the electrons traveling between n and $n+1$ dynodes. For uniform potentials between dynodes, the field at the n dynode is doubled. Thus the transit time between dynodes is about 2.6 nsec and the transit time fluctuation ε_{SS} is 10% or 0.28 nsec. The transit time fluctuation in the first stage of the multiplier ε_{S1S2} is much larger at about 0.90 nsec, due no doubt to the extreme difficulty of making geometric compensation for this stage.

The total transit time of a twelve-dynode conventional fast photomultiplier is 43 nsec and the total transit time fluctuation ε_{PH} is, by (14), equal to 0.60 nsec for a $g_1 = g = 4$. The single electron time response by (15) is 3 nsec if the anode does not broaden it and if the center of the photosurface is used. Some manufacturers quote a pulse response for full illumination of the photosurface and so include the photosurface transit time difference. Table IV

TABLE IV

SINGLE PHOTON TIMING (AND DETECTION) CHARACTERISTICS OF SELECTED PHOTODEVICES[a]

Photodevice type	Identification	Gain	Δ	Transit time	Time resolution R	Rise time T_r	Pulse width P
Photomultiplier with linear focused multiplier of electrostatic type	Amperex 56AVP	10^8	(1.5)	41	1.2	2	2.5
	Amperex XP1020	10^8	0.9	28	0.66	1.8	2.2
	Amperex XP1210	10^7	0.8	20	0.38	1	1.2
	RCA 8575	10^8	1 to (1.2)	31	1.1	2.1	—
	RCA C31000E/F	10^8	(0.6)	34	0.6/0.45	2.4	—
	RCA 8850	10^9	(0.4)	31	—	2.1	—
	RCA C31024	10^6	0.5	—	0.47	0.8	—
	RCA C31000K C31034	10^6	1.5	—	0.60	—	—
	RCA 31024B	10^6	0.6	—	—	0.8	—
	RCA C70045	5×10^6	0.8	34	0.32	0.45	0.84
Static crossed field	Sylvania 502	2×10^4	1.5	0.1	—	0.1	—
Channel photomultiplier	Bendix BX 754	10^7	(0.4)	2	—	—	10
	Amperex HR300	10^5	—	1	<0.2	—	<0.3

[a] All times in nanoseconds. R is the experimental time resolution and is related to the theoretical ε_{PH} by 2.36 ε_{PH}. P is the measured output pulse width and is related to λ by 2.36λ. Δ is the single photon pulse height resolution related to ε_A by 2.36 ε_A and is here usually theoretical unless noted by ( ). See text for references.

summarizes these time properties for the conventional fast photomultiplier as do Chevalier, Boutot, and Pietri (*55b*). A check of the $\sqrt{\varphi}$ dependence of (17) can be obtained by examining manufacturer data (e.g. *56*) on transit times. The φ dependence of the pulse width P (or the rise time) and hence the individual transit time spreads checks for only a few tubes with many being

closer to a $\sqrt{\varphi}$ dependence. Discrepancies may be due to the method of measurement since the whole photosurface may have been illuminated or the rise time measured using a sampling scope triggered by the light pulser. Two popular examples of this fast conventional photomultiplier are the Amperex 56AVP and RCA 8575 listed in Table IV.

b. Improved fast photomultipliers. The conventional fast photomultiplier discussed above has been improved as is evident in Table IV. Reductions in transit time spreads of the larger photosurface tubes were made by redesigning the configuration of the input optics and raising the accelerating potential of each stage. Pietri and Nussli (*5*) and Pietri (*33,54*) give a good view of the evolution of the three Amperex tubes in Table IV. Chevalier *et al.* (*55b*) give a concise tabulation of this evolution. The higher S1 potential and the new input optics created a much higher initial field at the photosurface (i.e. 5 to 6×) and better isochronism to S1 for edge photoelectrons, leading to an ε_{KS1} of about 0.07 nsec. The redesign of S1 and S2 in addition to the higher potentials (e.g. 3×) and multiplication factor (e.g. 9) reduced the ε_{S1S2}/g_1 contribution to (14) to 0.10 nsec. The ε_{SS} was reduced to about 0.13 nsec by the higher potentials and its contribution to the total transit time spread reduced to 0.03 nsec. Straightforward improvements to conventional tubes thus result in transit time spreads of about 0.13 nsec and experimental time resolutions R of as little as 0.38 nsec. The SER impulse response given by (15) was decreased to 1.2 nsec. It had been reduced not only by the reduction in individual spreads but also by the reduction of the number of dynodes from 14 to 10 and the use of a coaxial output line. A contemporary tube by RCA (i.e. C70045) achieved comparable speeds with a unique multiplier design employing interdynode accelerating and decelerating grids and with a side-looking large photosurface. This tube has been studied in detail experimentally by Birk *et al.* (*53*). The SER amplitude distributions of these improved tubes probably corresponds to a Δ of 0.83 due to the higher gains at the first dynode (e.g. $g_1 = 10$). These time resolutions and responses probably represent a lower limit that can be achieved with conventional materials, large photocathodes, and linearly focused, electrostatic multipliers.

A second approach to improving conventional large photocathode photomultipliers is to incorporate some of the new secondary emission material in them. The time resolution (14) should be improved by the higher g_1, the higher potentials used to obtain the g_1, and the lower velocity peak of the secondary electron distribution. RCA has placed such a high gain dynode in the first stage of the multiplier of the RCA 8575. This C31000E/F (or 8850) has been examined for time resolution by Present and Scarl (*57*) who find an improvement of 40% to 0.64 nsec. The increase in g_1 appears to account for the entire improvement. Lakes and Poultney (*58a*) reported an R of 0.45 nsec

for the same tube using a different technique and a wavelength much closer to the wavelength threshold of the photosurface (i.e. 0.4 eV vs 1.4 eV). A larger ε_{KS1} due to a higher W_n of photoemission in the former measurements may have masked the improvement in ε_{S1S2} due to the lower W_n of secondary emission. The latter measurement indicates the expected improvement for a lower W_n at the first dynode. The impulse response (15) would not be expected to change due to the initial stage improvements. To decrease this response in any multiplier and maintain the necessary gain, one could use a few number of high gain dynodes. RCA has reduced the number of conventional dynodes from 12 in the 8575 to 5 high gain ones in the C31024, increased the interdynode potentials by about a factor of 3, and added a coaxial output at the anode. This modification is reported to decrease the rise time of the impulse response from 2.1 nsec to 0.8 nsec. The corresponding P are 2.9 and 1.1 nsec if the output pulse is given by (4) since one can show that P equals 1.4 times the rise time. A decrease in P from (15), (16), and (17) to 0.9 nsec might have been expected for the potential increases and to 0.68 nsec for a drop in W_n to 1 eV. However, a rise time measurement with a fully illuminated photosurface may have masked the full decrease due to the transit time difference problem at the photosurface. Leskovar and Lo (*58b*) have just completed detailed studies of the RCA 8850 and C31024. They report time resolutions of 0.58 and 0.47 nsec, respectively, which may indicate that a geometric limitation in the KS1 region probably exists in these devices. The ultimate in time resolution and impulse reponse for large photosurface photomultipliers could probably be obtained by using high gain dynodes in the fastest conventional tubes discussed in the preceding paragraph. One might expect an ε_{PH} of 0.1 nsec and a λ of 0.2 nsec.

A third approach to improving the time resolution of conventional fast photomultipliers would be to give up the requirement of a large photosurface; which is quite feasible for many applications having narrow, collimated light signals. This relaxation can be done in a straightforward manner by placing one of the new photosurfaces on the "first" dynode of an existing multiplier structure. The total gain G_1 of the tube drops slightly and the ε_{KS1} no longer contributes. The relatively large ε_{S1S2} of the original tube now decreases (to about 0.3 nsec) by (16) and (17) since W_n is now that of photoemission, but the high g_1 is not present to allow a better sampling of that transit time fluctuation by (14). The author has found that the time resolution of such a tube (e.g. C31000K or C31034) based on the 8575 is quite close to the time resolution for the C31000E. A predicted time resolution of 0.35 nsec is not approached perhaps due to geometrical problems in the first stages now without the long KS1 stage. The additional use of high gain dynodes as in the RCA C31024B may or may not improve the time resolution depending on the

presence of the geometry problem. The reported rise time of the C31024B is 0.8 nsec which shows no improvement over the C31024 due to reduced spreads in the initial stages, but then Krall and Persyk (*55a*) indicate an anode design limitation. Measurements are needed on these new material photomultipliers to answer the above questions. If the input stages of the multiplier do place a geometrical limit on time resolution and impulse response, it is probably more effective to place the small photosurface on one of the symmetric dynodes of the conventional multiplier (Fig. 3), replace the others with high gain dynodes, and inject the light from the side.

The use of a small photosurface of the new materials allows one to consider other fast multiplier structures. One such structure was developed for the RCA C70045C by Morton, Matheson, and Greenblatt (*59*). The addition of a photosurface on its "first" dynode might be expected to lead to an ε_{PH} of about 0.05 nsec. With high gain dynodes, this ε_{PH} might be reduced to 0.02 nsec and the practical operation of the tube considerably simplified. These transit time fluctuations are already near the expected emission times of the photoelectrons and secondary electrons. Only experiment will resolve the question of what the time resolution is and what its limit is. A second multiplier design is described by Miller and Wittwer (*60*) who use a "cancellation-in-pairs" geometry. They built and tested an eight stage version which exhibited performance comparable to the crossed-field photomultiplier discussed immediately below. Their measurements were consistent with an ε_{PH} of 0.01 nsec and an impulse response P of 0.07 nsec. It is not known whether the new materials would or would not improve this multiplier.

2. *Crossed-Field Photomultipliers*

Miller and Wittwer (*60*) also designed and built a photomultiplier which employed crossed electric and magnetic fields in conjunction with a segmented strip multiplier. The photosurface occupied one segment of the strip. The orbits of all electrons originating from rest on a given segment are congruent. These orbits are cycloids along the strip and strike where they will on the next segment. The transit time fluctuations arise solely from the distributions in emission velocities and are independent of the initial position at all electrodes. These fluctuations can also be represented by (16) where φ is about 3000 V for each stage. An eight-stage version was tested and achieved a gain of 10^5 and a frequency response of 4 GHz. These measurements were consistent with an ε_{PH} of 10 psec and a λ of 140 psec. Meiling and Stary (*3*) on p. 32 mention a Russian crossed-field tube and a prediction that its ε_{PH} could

be expected to be an order of magnitude better than conventional photomultiplier designs. The Sylvania 502 is a commercially available version with a gain of 2×10^4, 9 stages, conventional materials, impulse response P of 0.3 nsec, and an ε_{SS} of less than 10 psec. The gain cannot be raised once the magnetic field is selected and incorporated and so present versions may not be able to detect single photons. The higher gain, continuous strip, crossed-field multiplier mentioned in Section II,B,4 has also not been studied. The single photon detection and timing properties of crossed-field photodevices should be closely examined for they represent the ultimate in time resolution (e.g. $\varepsilon_{PH} = 10$ psec) and in impulse response (e.g. $\lambda = 70$ psec) among all the photodevices discussed in this review.

3. *Channel Photomultipliers*

The excellent single photon detection properties of the channel photomultiplier have already been noted for the Bendix BX 754. Studies of the single photon time resolution of this channel photomultiplier are not yet available in the literature. Estimates of its time resolution and impulse response can be made using Eqs. (13) through (17). A straight, electrostatic channel depends on the secondary emission velocity to cause the axially-accelerated electrons to hit the opposite side of the channel and multiply. For a W_n of 3 eV, a channel diameter of 1 mm, and a channel length of a few centimeters, one concludes that the transit time between multiplications is 0.9 nsec, the total transit time is about 9 nsec, and the ε_{SS} is 0.9 nsec. The ε_{KS1} and ε_A are separate problems. A typical φ_{KS1} is 200 V and the "s_1" is 1 mm. ε_{KS1} is then 4% of t_1, by (16), or about 0.02 nsec. Additional transit time spreads may enter due to delay variations of about 0.2 nsec which depend on the point of impact of the photoelectron and variations which depend on pulse saturation. Omitting these and any anode problem, one might expect an ε_{PH} of 0.45 nsec and a λ of 2.7 nsec. Boutot and Pietri (*20*) report that the microchannel wafer they studied would be expected to have ε_{KS1} less than 10 psec and ε_{SS} less than 100 psec. Careful design at the input and output was necessary to preserve its time resolution. Pulse responses less than 300 psec were expected (evidently nonsaturated operation), but the test light source allowed only the conclusions that it was less than 500 psec. Total transit times of 1 nsec were expected. Gains of 10^5 were achieved. Chevalier *et al.* (*55b*) measured a single photon time resolution of less than 0.2 nsec for this HR300 microchannel photomultiplier, but were probably limited by the method used.

B. Time Derivation and Time Interval Measurement Circuits

1. Time Derivation Circuits

In order to time intervals to high resolution, the arrival time of the single photon anode pulse must be determined by a suitable detection circuit, also called a time pickoff circuit or timing discriminator. This timing discriminator also acts as an integral pulse height discriminator but any simultaneous pulse height measurement or selection should be done in a separate slow channel. Its output is a standard fast pulse for further processing. A variety of timing discriminators have been developed for timing with fast scintillators and are described by Meiling and Stary (*3*) in Section 3.4.2, by Kowalski (*1*) on pp. 179 and 217, and by Gedcke and McDonald (*61*). Three of these techniques are leading edge timing, fast crossover timing, and constant-fraction-of-pulse-height timing. Leading edge timing gives excellent results for anode pulses within a narrow pulse height range. Miehe, Ostertag, and Coche (*62*) measured a time resolution of 76 psec using the C70045 photomultiplier, a fast leading edge timing discriminator, and a fast light pulser producing a short, multi-photon signal. This time resolution probably represents the capability of the timing discriminator for a pulse height range of about 10% since the large signal (e.g. 400 photoelectrons) reduces the transit time fluctuation of the photomultiplier (13) by about a factor of 20 through better sampling of the KS1 region. The leading edge timing discriminator produces an output pulse at a time (often called the machine time) related to the instant at which the anode pulse crosses a certain pulse height threshold, Fig. 8. Its time resolution can be limited by a number of factors. The most important is the walk effect. Pulses with the same rise times but different amplitudes cross the threshold at different times as shown in Fig. 8. The walk effect becomes especially bad at the single photon level where the pulse height fluctuation is characterized by $\varepsilon_A{}^1$. The resultant timing uncertainty can be expressed as ε_t given by

$$\varepsilon_t = \varepsilon_A{}^1/(dA(t)/dt)_{t=T}, \tag{18}$$

where the denominator is the slope of the average signal shape $A(t)$ as it crosses the discriminator threshold at $t = T$ and $\varepsilon_A{}^1$ equals A times the relative variance ε_A previously used. An approximate ε_t for the walk of single photon timing can be obtained from (18) in terms of the width of the SER amplitude distribution Δ and rise time T_r of the photomultiplier by considering the leading edge of the anode pulse to have a linear rise. In this approximation,

$$\varepsilon_t = \varepsilon_A T_r = \Delta T_r/2.37. \tag{19}$$

For wider ranges of amplitudes, this approximation does not hold and the timing uncertainty increases more rapidly. The walk effect can be minimized

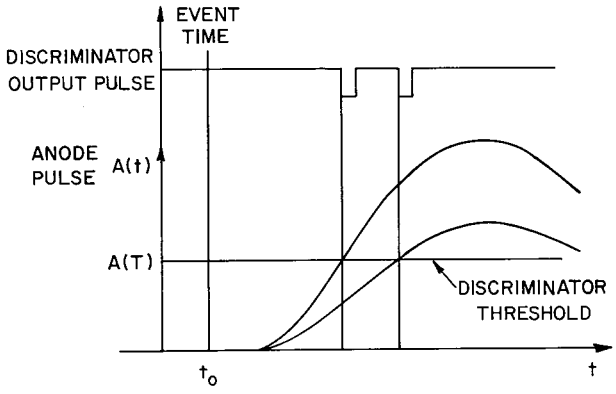

FIG. 8. The walk effect in leading edge timing discriminators due to variation in pulse height amplitudes. Walk due to charge sensitivity of the discriminator has been omitted. (Courtesy of Ortec, Inc.)

by using photomultipliers with fast rise times and narrow single photon pulse height distributions. For example, the RCA 8850 in Table IV would show an additional timing uncertainty ε_t due to walk in a leading edge discriminator of 0.35 nsec for a single electron counting efficiency of 84% and 1.6 nsec for about 97% efficiency. The general references for this section describe other methods for correcting this walk effect. The simplest is selection of a narrow range of pulse heights by means of a slow parallel channel (see Section II,B,2), but this cannot be used if one requires high counting efficiencies.

Fast crossover timing and constant-fraction-of-pulse-height timing were developed to overcome the serious walk effect in the wide dynamic range use of leading edge timing. In fast crossover timing, the anode pulse is clipped to produce a bipolar pulse with a zero crossing. A fast crossover discriminator is used as the timing discriminator. The zero crossing time represents the same phase point on all pulses and the walk effect is nearly cancelled. This method provides good walk characteristics over a wide range of pulse heights (e.g. less than ± 100 psec for 100:1 dynamic range) (*61*). For a narrow dynamic range, its time resolution is somewhat worse than with leading edge timing. In constant-fraction-of-pulse-height timing (*61*), an attenuation-subtraction shaping technique is used to produce the pulse with a zero crossing phase point. Its walk characteristics are typically less than ± 120 psec for a 100:1 dynamic range and its time resolution is comparable to that of leading edge for narrow dynamic range. The zero crossing phase point was selected to be on the leading edge of the anode pulse because studies of leading edge timing with scintillators (e.g. *63*) showed that the time resolution was a function of the fraction of the pulse height used as the threshold. The optimum triggering level varied between 10% and 20% depending on the light

source. Constant-fraction-of-pulse-height timing has the advantage over fast crossover timing that these small fractions can be attained. Fast crossover timing is found to work best for fractions near 50% due mainly to noise and ringing on the tail of the anode pulse. The optimum fraction is thought to occur because of finite rise times of scintillator light pulses. The author has not found any clear evidence for an optimum fraction with single electron pulses.

The above timing discriminators have a number of common problems. Electrical noise will cause a jitter in the timing, based on (18). The faster the rise time from the photodevice, the smaller the jitter will be. If a fast amplifier must be used due to total gain considerations, there will usually be an optimum rise time since circuit noise increases with amplifier bandwidth. Any time jitter in the anode pulse will be passed directly on to the processing circuit. An additional walk not shown on Fig. 8 is a walk due to the charge sensitivity of the timing discriminator. This finite charge threshold can be represented by equal areas under the anode pulse and therefore adds a different walk for each pulse height. Tests of commercial fast timing discriminators with electrical test pulses indicate that this walk is usually a much smaller effect than the walk discussed above. Finally, it has been assumed above that the anode pulse has a constant shape. If this assumption should not hold in a particular application, an additional walk due to varying rise times would enter in both leading edge and fast crossover timing. Constant-fraction-of-pulse-height timing has been shown by Chase (*64*) to be adjustable so as to cancel this rise time walk.

The determination of the arrival time of the photodevice output pulse for further processing is one of the limitations to fast timing, especially for single photon pulses of varying amplitude. This range of pulse heights can be minimized by the choice of a photodevice with a narrow SER amplitude distribution Δ from Table IV. The promise of the channel multiplier is that operation in the saturation region might further narrow Δ below 0.4 so that only a leading edge discriminator need be used to realize its inherent timing precision. Tests of commercial fast discriminators with standard electrical pulses indicate that they are capable of precisions of 10 psec. In timing one need not preserve all the pulse height information as is most evident in the channel multiplier. It is worth the try to see if saturation can be used in photomultipliers to limit the range of pulse heights without introducing varying transit time delays due to the saturation. In most cases, however, constant-fraction-of-pulse-height timing is the choice. This method has been used in most of the test methods described in Section III,C,1. The measurements by Gedcke and McDonald (*61*) in their Fig. 4 give an idea of its precision over pulse height ranges smaller than 100:1. For example, a selected 4:1 range would probably yield ± 50 psec or better. Leskovar and Lo (*58b*), on the other hand, favor fast crossover methods for single photoelectron timing.

2. Time Interval Measurement Circuits

Now that a standard timing pulse is available for each event of interest, the time interval between two such events must be measured to the precision required. Kowalski (*1*) in Chapter 5 and Meiling and Stary (*3*) in Section 3.4 describe a wide variety of time interval measurement techniques. Only two techniques will be discussed in this review; a technique for intervals shorter than tens of microseconds here and a technique for intervals up to seconds in Section III,D,2. The short interval measurement can be done using a time-to-pulse-height converter capable of 0.02% or better resolution in ranges as small as 50 nsec. Typical circuits are shown in Figs. 9 and 10. During the interval between start and stop pulses a capacitor is charged from a constant current source. The amplitude of the voltage generated on the capacitor is linearly related to the time interval between these pulses and is read into the memory of a multichannel pulse height analyser for later use. The start and stop pulses can be obtained from the same photodevice if they occur far enough apart, from two photodevices, or from one photodevice and an electrical sync signal. Higher data rates could be obtained with a number of stop channels going to their own time-to-pulse-height converter which is started by a single sync pulse. However, the readout system quickly gets very sophisticated. All of the diagnostic work on photodevices and circuits and all of the applications involving short time intervals which are discussed below make use of the time-to-pulse-height converter technique.

A typical processing delay in the time-to-pulse-height converter is one microsecond. If such a delay does not affect the application, the time-to-pulse-height converter can be used as a coincidence circuit to provide information that the events occurred within a certain interval of each other. This mode of operation requires a single channel pulse height analyzer with its window properly set. A second single channel analyzer can be set to monitor the random coincidence background. The narrower the window, the more inefficient the counting becomes. If fast information must be provided about the coincidence of two events, fast coincidence circuits must be used entirely as discussed in the general references above. An additional important application of slow single channel analyzers and coincidence circuits is their use to select either desired pulse height ranges in one or both time-to-pulse-height channels as outlined in Fig. 12. The single channel analyzers view a slow, linear pulse from one of the last dynodes when photomultipliers are used. If the pulse heights are in the desired range, the single channel outputs produce a slow coincidence signal in a coincidence circuit which gates the multichannel analyzer to view the time-to-pulse-height converter output. This fast/slow scheme can be used to select single photon events with photodevices possessing good pulse height resolution or to minimize the walk due to a wide range of anode pulses.

C. Single Photon Timing Methods

1. Introduction

Single photon precise timing experiments make use of all the time derivation and interval measurement circuits described above. It is very important to be able to carry out diagnostic studies on the time resolution of the photodevices used as well as on the stability, time resolution, and calibration of the timing circuits. The diagnostic studies will employ circuit configurations almost identical to those of the experiments themselves except for the introduction of test light or electrical pulses at the appropriate points. These circuit configurations are of two general classes. The first class makes use of a low jitter electrical signal synchronous with a short light pulse as the start pulse as shown in Fig. 9. For a very weak light pulse with width much shorter than the photodevice transit time fluctuation, the result is a measurement of the single photon transit time fluctuation of the device. The second class of

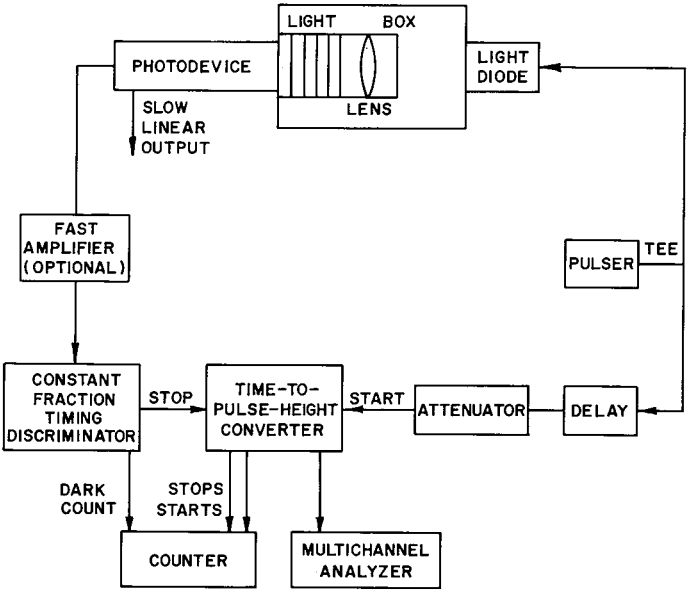

FIG. 9. General block diagram of the electronics for single photoelectron time resolution measurements of a photodevice using an electrical start pulse. The light box had a shutter and an inner box with slots for various optical filters and attenuators. The lens was used to illuminate only a small portion of the photosurface. The counter was used to monitor photodevice dark count rates and the start and stop rates of the time-to-pulse-height converter.

diagnostic studies of a photodevice makes use of photodevices in both channels as shown in Fig. 10. For a very short, weak light pulse, the result is a measurement of the convolution of the transit time fluctuation of both photodevices. If the light source in Fig. 10 allows one of the photodevices to operate at high light levels or if one of the photodevices is much better than the other, the second class of diagnostic studies approaches the first in practice. The realization of light pulsers with the above properties (i.e. single photons within tenths of nanoseconds and an electrical sync pulse) is not an easy matter and is discussed first in Section III,C,2. The electrical tests for circuit time resolution, calibration, and stability are a good deal easier and are discussed in Section III,C,3. A brief view of other diagnostic studies of a photodevice (e.g. impulse response) is given in Section III,C,4.

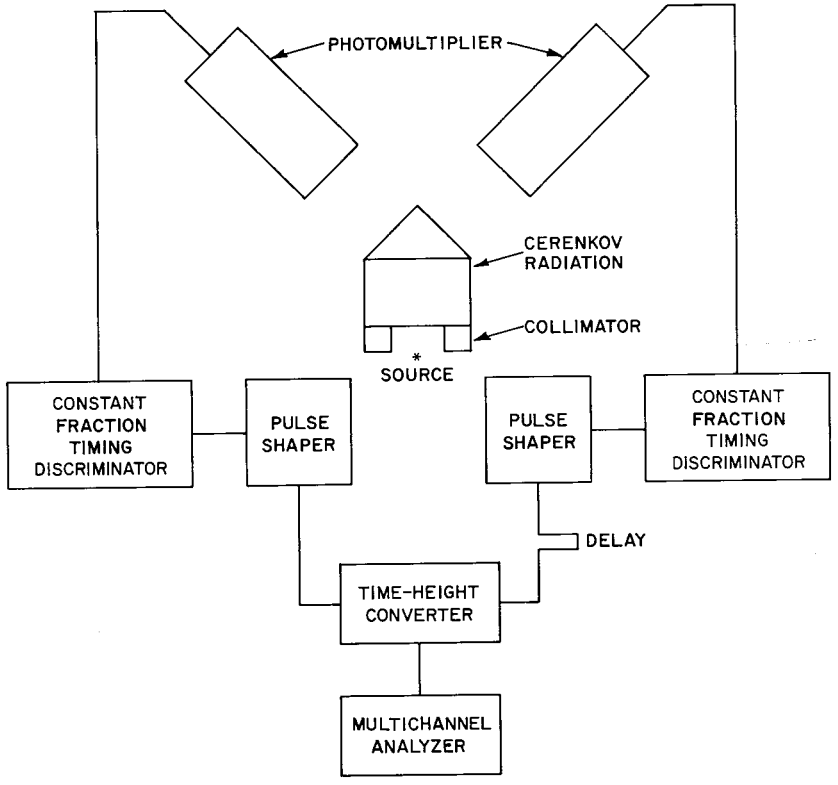

FIG. 10. General block diagram of the electronics for single photoelectron time resolution measurements of a photodevice using two photodevices. The radioactive source emits particles which radiate light in the Cerenkov radiator. Other light sources could be substituted. From Present and Scarl (*57*). (Courtesy American Institute of Physics.)

Measurements of the single photon transit time fluctuation consist of viewing the pulsing light source with either the circuit in Fig. 9 or the one in Fig. 10 and of accumulating the distribution on the multichannel pulse height analyzer. Its full width at half-maximum in Fig. 11 is the R used above. Figure 9 also allows a measurement of the transit time of the photodevice. It is here assumed that the walk effect has been eliminated in a suitable

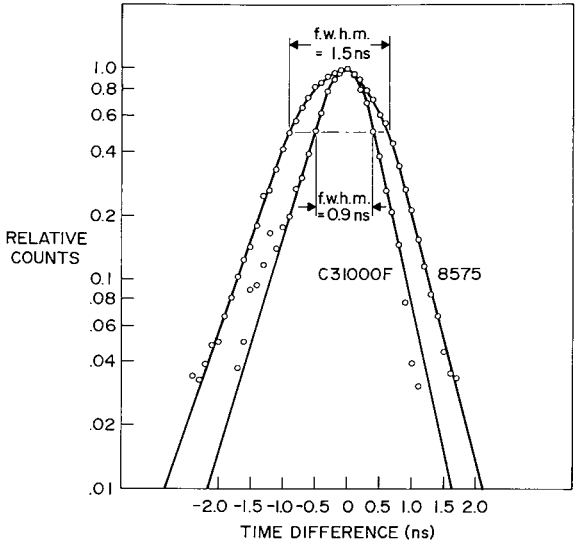

FIG. 11. Measured time difference distribution for pairs of photomultipliers responding to simultaneous single photons using the circuit of Fig. 10. The outer curve is for a pair of tubes with CuBe first dynodes, the inner for a pair of tubes with GaP first dynodes. Present and Scarl (*57*). (Courtesy American Institute of Physics.)

fashion and that the light pulser emits very short pulses consisting of single photons. Adjustment of the light pulser to give these single photon signals is closely related to the ability of the photodevice to detect single photons. To separate the two, one might repeat the procedure outlined in Section II,D with a steady, weak source, but with no other changes in the circuits. One might rather choose to use the light pulser itself and look at the pulse height spectrum of linear pulses detected using Fig. 9, especially if a high device noise causes problems with the method of Section II,D. If the photodevice under study has excellent pulse height resolution, one merely attenuates the light pulse in a suitable fashion until the multielectron peaks go away and adjusts the system gain so that the single electrons are detected. For wide SER amplitude fluctuations or saturated pulses, an indirect technique must be employed. This technique was first used by Tusting, Kerns, and Knudsen

(*65*) to ensure that only a single photoelectron is emitted for each light pulse. It will now be assumed that the light pulser generates a pulse constant in shape and intensity as well as being sufficiently short. It will be shown in Section IV,B that the probability of detecting r photoelectrons, P_r, in a single flash when m is the number expected on average is well described by a Poisson distribution for coherent or broadband light.

$$P_r = m^r e^{-m}/r! \tag{20}$$

The mean number of photoelectrons expected, m, can be shown to be just the mean number of photons multiplied by the total counting efficiency of the photodevice. The probability of detecting no electrons in a flash P_0 is then

$$P_0 = e^{-m} = 1 - \delta, \tag{21}$$

where δ is the probability of detecting an event. The probabilities P_1, P_2, etc. can be generated from P_0 by use of the relation

$$P_{r+1}/P_r = m/(r+1). \tag{22}$$

If now the light pulse is attenuated until very few flashes are detected as stops (e.g. the fraction δ), m approaches δ, P_1 approaches m, and the probability of detecting other than single electrons vanishes. Table V gives these probabilities for various fractions of the flashes detected. A δ of 10% or less is typical in a totally blind situation and thus makes the technique quite inefficient unless a high pulse rate is available. Included in Table V are the probabilities of occurrence for higher δ. If one can resolve the multielectron pulses in an auxiliary channel and eliminate them from the analysis by gating off the multichannel analyzer, one can greatly increase the data rate of the measurement. The maximum occurrence of single electron pulses is 37% of the light pulse rate at a detection rate of 63%.

The use of a light pulser makes it possible to dispense with dark noise reduction techniques in many cases. One usually works on the 50 nsec range of the time-to-pulse-height converter which only registers noise counts that are in coincidence with signal counts within this range. If a start rate of 700 Hz is available and a δ of 10% used, a dark count rate of 30 kcounts/sec will yield only one accidental count per second while the detected stop rate will be 70 Hz. A final check of both photodevice and light pulser adjustments for single photon counting can be made in the totally blind version of Fig. 9. The optical attenuation can be varied in known steps and the stop rate checked to see if it is a linear function of that attenuation. This test follows directly from (21) for small m.

If the test circuit of Fig. 10 is used where both photodevices must operate on single photons, it is probably best to locate the single electron counting plateau separately for each photodevice using the test circuit of Fig. 9. To

TABLE V

THE PROBABILITY OF OCCURRENCE OF SINGLE AND MULTIPLE PHOTOELECTRON PULSES WHEN THE PHOTODEVICE IN FIG. 9 DETECTS ONLY THE FRACTION δ OF THE LIGHT PULSE RATE[a]

		r			
δ	m	0	1	2	3
0.01	0.01	0.99	0.01	0.0005	—
0.05	0.05	0.95	0.05	0.001	—
0.10	0.10	0.90	0.094	0.005	—
0.20	0.16	0.80	0.18	0.02	—
0.40	0.51	0.60	0.30	0.08	—
0.60	0.91	0.40	0.37	0.16	0.05
0.80	1.6	0.20	0.32	0.26	0.14
0.90	2.3	0.10	0.23	0.26	0.20

[a] Mean number of photoelectrons is also given for each δ.

ensure that the short light pulse of Fig. 10 contains only a few photons, one can examine the pulse height spectrum of each photodevice and if they possess good resolution attenuate as necessary. Where pulse height discrimination is not possible, one must use the indirect method described above. At best, one photodevice can be strongly coupled to the light pulser in turn and the other one adjusted for single photon operation. To count single photons in both channels, the so determined optical attenuation is added to both channels at once. In practice, the count rates will be quite small (e.g. 1 count/sec) and accidental noise counts will become serious if the photodevices do not have noise reduction provisions. Surprisingly, it will be shown below that the circuit of Fig. 10 can be used with a filtered thermal light source to measure the transit time fluctuations of photodevices.

2. *Light Pulsers for Testing Photodevices*

Light pulse generators may be divided into two classes; those with light pulse widths much shorter than the photodevice transit time fluctuations under study and those with light pulse widths comparable to or larger than these fluctuations. The latter are very convenient to use and may in special circumstances allow a statement about transit time fluctuations. A third class of light source is the steady, filtered thermal source.

a. Very short light pulse generators (100 psec or less). Light pulses with widths smaller than 100 psec are available from mode-locked, pulsed lasers either in a pulse train or a single pulse. DeMaria, Stetser, and Glenn (*66*)

give a general review of this technique and Carman, Reintjes, and Furumoto (*67*) give a recent account of single pulse production, These single pulses typically occur at very low repetition rates, in the green if frequency-doubled Nd:YAG, and with about 10^{16} photons. The pulse trains typically yield pulses too close together to be used in the manner of Fig. 9. These features make the use of this light generator for transit time fluctuation studies very inefficient and expensive. The real value of this light pulse generator for testing photodevices comes in other diagnostic studies such as measurements of impulse responses.

Fortunately for the worker of modest means, there is a second means of producing these very short light pulses, which makes use of the Cerenkov radiation process. This weak radiation is emitted over a wide spectral range by a charged particle traversing a transparent medium above a threshold velocity. Scarl (*68*) used a 100 μCi $Sr^{90}Y^{90}$ source to produce Cerenkov light in plexiglass as shown in Fig. 10. The electrons from the beta decay have a maximum energy of 2.2 meV, a maximum range of about 1 cm, and are collimated to a narrow beam before entering the plexiglass. Each electron produces at most 50 photons in the wavelength interval between 3000 and 7000 Å. The radiator is designed so that these photons leave the plexiglass simultaneously limited only by dispersion in the plexiglass (e.g. 5 psec). With the photocathodes of the two PMT about 13 cm away from the radiator, most of the photons produced by each beta particle go undetected. However, two photons produced by one particle do hit the two cathodes often enough to give a coincidence rate of about one event per second. After a running time of hours, the time distribution on the multichannel pulse height analyzer looks like Fig. 11 which shows the convoluted transit time fluctuations of two pairs of photomultipliers respectively. Time jitter in the electronics of Fig. 10 is believed to contribute less than 0.1 nsec to this time spread in the worst case. In addition, only the central 2.5 cm of each photocathode was illuminated to eliminate any photosurface transit time difference problems.

Lami, D'Alessio, Zampach, Radicella, and Kesque (*69*) have recently constructed a clever modification of the Cerenkov light pulser in which one channel produces a low jitter start pulse. The Cerenkov radiator is modified so that the charged particle escapes from the radiator and produces a large light pulse in a fast scintillator attached to the start channel photodevice. Only the stop channel views the single photon Cerenkov signal. The resultant timing curve gives the transit time fluctuation directly. A resolution R of 1.61 nsec was quoted for an Amperex 56 UVP, but the walk effect may have been overlooked. These workers were involved in the study of the short decay times of fluorescence induced in scintillators by ionizing particles as discussed in Section III,D,1.

The data rates of the Cerenkov pulsers are quite low for a variety of reasons and require moderately long data runs. Practicality aside, perhaps the most useful Cerenkov pulser would consist of two radiators placed in a monoenergetic, collimated beam from an accelerator which consists of one particular type of particle at an optimum velocity. The start channel of the test circuit would be closely coupled to its radiator while the stop channel would be weakly coupled.

b. Short light pulse generation (0.5 nsec and longer). Short light pulses of about the width of the transit time fluctuations under study can be conveniently produced in three basic ways. Either a short electrical pulse can feed a suitable lamp, an energetic charged particle can excite fast fluorescence in a suitable medium, or a continuous gas laser can be mode-locked. Kowalski (*1*) on p. 52 gives a list of references for a number of these light generators. Meiling and Stary (*3*) briefly review them in Sections 2.2 and 4.2 and on p. 377, as well as reviewing test methods with these light generators in Section 4.4. The mode-locked laser is again most useful for the other diagnostic studies. The use of fast scintillators is mentioned in conjunction with Section III,D,1. The use of a pulsed lamp is especially convenient for testing preliminary to a precise measurement of transit time fluctuation in a photodevice. Here only the use of inexpensive, light-emitting semiconductor diodes will be described. The short pulser based on this device consists of two parts; an electrical pulser which produces the necessary short electrical pulse and the light diode which can follow the fast electrical pulse. The fast electrical pulser is itself a necessity for testing and calibrating the fast circuits and components discussed above. A well-known pulser for these purposes is the Tektronix 109 mercury reed pulser which has rise times less than 0.25 nsec, minimum full width at half-maximum of 0.5 nsec, repetition rate of about 600 Hz, and amplitudes up to 50 V. Lakes and Poultney (*58a*) used this pulser to drive a GaAs red light diode in their study of the transit time fluctuation of the RCA C31000E as sketched in Fig. 9. They also used a pulser built by a colleague which was triggerable, operated at higher repetition rates (e.g. 10 kHz), and had a full width half-maximum of 0.3 nsec. It consisted of a step recovery diode which shaped a relatively slow trigger pulse, an avalanche transistor fired by the shaped pulse, and an open-ended transmission line which was thereby discharged into the light emitting diode. The exact shape and width of the light pulse is not yet known, but the light pulse is fast enough to study transit time fluctuations greater than about 0.5 nsec.

If the shape of the short light pulse is either known or can be measured, it is possible to unfold the photodevice time resolution from the observed distribution. Measurement of the shapes of weak short light pulses is discussed in Section III,D,1 and presupposes the availability of a photodevice

with a transit time fluctuation shorter than the one under study. The shapes of strong short light pulses can be measured using fast semiconductor diodes, streak cameras, and nonlinear optical techniques. The mercury switch pulser used by Birk *et al.* (*53*) probably fits into the category of a known light pulse in that it behaved as if it were exponential decay of 300 psec with a much shorter rise time. Koechlin (*70*) was probably the first one to use the method of Fig. 9 to measure the single photon transit time fluctuation of a photomultiplier. Koechlin and Raviart (*71*) review this method and show that their result for a 56TVP is compatible with an unfolding from the observed shape of a fast scintillator decay which is assumed to be exponential. They used a mercury switch with similar time characteristics to the above one, but obtained a single photon time resolution R of 0.6 nsec for the 56 TVP which is at least a factor of two shorter than observed by other workers. Birk, Kerns, and Tusting (*53*) were, of course, measuring a faster photomultiplier and used the unfolding technique on the light pulse shape itself. One other known light pulse shape that should be considered for these measurements is the nearly square wave shape of the injection-laser diode mentioned in Section III,C,4.

c. Filtered, thermal light source. The intensity of a filtered, thermal light source fluctuates on a time scale of the order of magnitude of the inverse of the spectral frequency width as discussed in Section IV,B. Given the spectral width, one can compute the correlations in the photon arrival times. For example, a 1.6 GHz mercury line would yield a distribution 0.17 nsec wide. Scarl (*68*) measured this distribution using a circuit similar to that in Fig. 10. The distribution is significantly affected by the transit time fluctuations of the photomultipliers. Scarl built the Cerenkov light source in order to take these fluctuations into account. Now that the phenomenon is understood, his experiment can be turned around and used to measure the transit time fluctuations of a pair of photomultipliers. The experiment is quite difficult, though, as discussed in Section IV,B,3 and takes an order of magnitude longer than the measurement with the Cerenkov source.

3. Calibration and Stability of Timing Circuits

It is important for fast timing to use stable, low jitter circuits and components and to be able to calibrate and monitor these at will. The key to the precise measurement of short time intervals discussed here is the time-to-pulse-height converter which includes the multichannel analyzer as one unit. It should be carefully calibrated and monitored. Measurement of its differential and integral nonlinearities is mentioned by Kowalski (*1*) in Section 5.5 and Meiling and Stary (*3*) in Section 4.4.6. Differential nonlinearity is the deviation of channel widths from a nominal value and is measured by feeding

the start and stop channels with uncorrelated pulses. Integral linearity is the correspondence of each channel to the time difference of the events and is often measured with delay lines and pulse generator. Probably the most sophisticated calibration and monitoring scheme has been used for the Lunar Ranging Experiment in which a 2.5 sec interval must be known precisely and accurately to 1 nsec or better as discussed in Section III,D,2. This scheme, capable of an accuracy of 0.1 nsec, has been described by C. Steggerda of the University of Maryland in an unpublished report. One part of it is based on the precision crystal oscillator in the timekeeping system of the experiment. The oscillator output is multiplied to 20 MHz and sent to a fast leading edge discriminator to produce standard timing logic pulses to operate the time-to-pulse-height converter or other circuit components. If these timing pulses are sent to both start and stop channels, the multichannel pulse height analyzer would show a peak on its time axis at 50 nsec. The remaining time axis interval of 0 to 100 nsec is calibrated using a family of delay cables specially constructed for this application. As a first approximation, the delay cables can be cut to appropriate lengths calculated from the advertised propagation speed. Precise adjustments can be made based on extensive intercomparisons of the cable family using the 20 MHz pulse rate and a fast oscilloscope as a null detector. Meiling and Stary (*3*), in Section 4.4.5, and Taylor (*72*) discuss other methods of cable calibration. Members of this delay family (e.g. a 10 nsec one) can then be alternately added first to the start channel and then to the stop channel to determine a time point below and above the 50 nsec point (e.g. 40 and 60 nsec). In the Lunar Ranging Experiment, the calibration of the time-to-pulse-height converter system is semiautomatic with data readout done by an on-line computer which also can calculate the best fit calibration curve.

Longer time intervals can be calibrated to the same accuracy by using a time delay generator in conjunction with a dual coincidence unit to gate any two clock pulses out of the clock pulse train. One thus has standard timing pulses available with a separation of 50 nsec up to a maximum of 2.5 sec. These standard pulses in conjunction with the calibrated time-to-pulse-height converter can be used for all other electronic diagnostic studies. In the lunar ranging system, moreover, these timing pulses can each drive a light emitting diode at the start photomultiplier and the stop photomultiplier for an integral system check in both precision and accuracy. Needless to say, most workers use simpler schemes such as displacing their timing peak along the time axis by a delay cable of 2 or 4 nsec.

4. Other Diagnostic Techniques

Fast counting with photodevices depends on the impulse response of the photodevice and the absence of correlated afterpulses. Neither of these

factors has a serious effect on short time interval measurements unless the same photodevice is used to provide both start and stop channels as in one class of photon statistics experiments discussed in Section IV,B. Due to this close relation, measurements of time correlated signals and noise in a photodevice are outlined there. Minor effects on time interval measurements have been reported due to the prepulsing in some photodevices mentioned in Section II,C and to a late peak observed in photodevice time resolution measurements. Yates and Crandall (*73*) mention one 25 nsec after the main peak. A possible cause could be prompt afterpulsing following a single photoelectron that was not detected by the stop channel.

Three methods of measuring impulse response deserve to be mentioned. Birk *et al.* (*53*) use a multiphoton Cerenkov light pulse to illuminate the photodevice and measure the impulse response in real time with a fast oscilloscope. Boutot and Pietri (*20*) used the pulse train from a mode-locked laser to measure the impulse response of their microchannel photodevice in real time with a fast oscilloscope. Miller and Wittwer (*60*) set an upper limit on the impulse response of their fast device using a mode-locked continuous gas laser in conjunction with a sampling oscilloscope. The single pulse mode-locked laser holds considerable promise for studying the transit time spreads in the stages of a photodevice in a step-by-step analysis. Most dynode materials are also photoemissive so that the laser can be used to inject an electron into a multiplier chain at a particular dynode. Finally, for those workers who like to measure the rise time of a device, at least one company is offering semiconductor laser diodes with a square shaped pulse of rise time less than 0.2 nsec. Many of the above diagnostic techniques are described in a recent supplement to the *IEEE Standards* [i.e. Adelman (*29*)].

D. Single Photon Precise Timing Experiments

Two basic types of single photon precise timing experiments will be discussed. The first type measures a fast decay time of an excited state by the single decay particle statistical technique outlined in Section III,D,1. The second type measures the time of flight of a light pulse to a distant target and back. Both types make use of the circuits discussed in Section III,B with the addition of a digital time interval measurement in the second case.

1. The Measurement of Lifetimes of Excited States

The fast decay time of an excited state can be measured by timing the appearance of a decay product after the excitation occurs in a statistical fashion. The excited state can be prepared by particle bombardment, flash lamp excitation, or decay of another excited state. The excited state under

study can be that of a nucleus, atom, ion, or molecule. The timing circuits are essentially those of Figs. 9 and 10 with sophistications added as shown in Fig. 12. The initial use of these circuits was made in the measurement of the decay times, schemes, and energies of excited nuclear states. The decay products were detected by converting all or part of their energies into fluorescent light in scintillators viewed by photomultipliers. The photomultipliers were operated at high light levels and the circuit time resolutions were complicated by the energy transfer process in the scintillator. These nuclear experiments would not be discussed (as they are briefly in Section III,D,1,d) if it were not for the fact that they have set the terminology, the theory, and some applicable results for single photon timing.

In the nuclear and atomic applications of these techniques, the number of decay products is very small after each excitation. The observed time distribution after a large number of repeated excitations would be expected to mirror the decay curve of the excited state. If more than one decay product is detected per excitation, this distribution would become skewed toward apparent shorter decay times. Bollinger and Thomas (*74*) were the first to apply this single decay product statistical technique to bright light flashes by attenuating the light signal until less than one photoelectron was detected in the stop channel per excitation, in much the same manner as described in Section III,C,1. They used slow timing circuits to measure scintillator decay

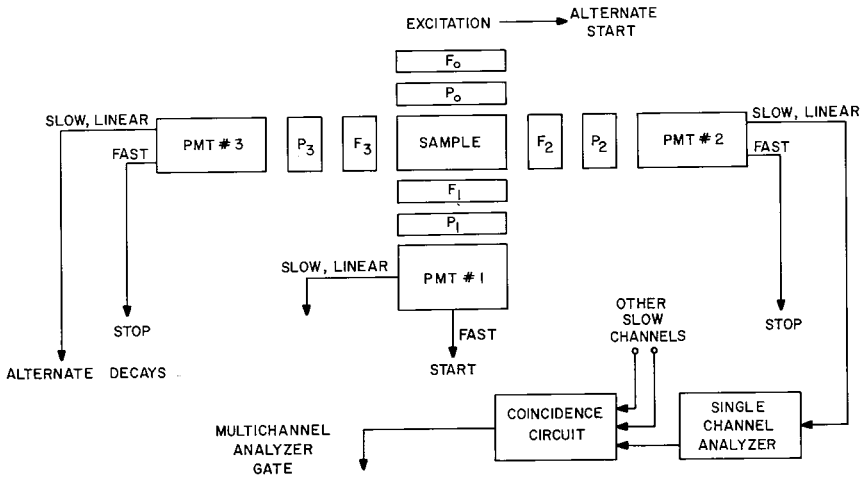

FIG. 12. General block diagram of the detection layout for the measurement of excited state decay times using the single photon statistical method. The electronics of Fig. 10 would also be used. Provisions are made for alternate decays, pulse height selection in a slow, linear channel, spectral selection by filters, F, and polarization selection by polarizers, P.

curves out to 30 μsec with a resolution of 6 nsec and were not affected by impulse response ringing and afterpulsing. Koechlin was probably the first to realize that this single photon technique could be used to measure much faster decay times (e.g. 2 nsec) with a resolution limited only by the transit time-fluctuations of the photodevice as outlined by Koechlin and Raviart (*71*). This single photon technique has recently been justified on the basis of the photon counting statistics discussed in Section IV,B,2 by Miehe, Ambard, Zampach, and Coche (*75a*). The shape of the light flash is represented by

$$J(t) = ni(t), \tag{23}$$

where n is the mean number of photons per flash and $i(t)$ is the probability density function of finding a photon at the photosurface at time t. The probability of observing the rth electron at time t, $P(r, t)$, is a product of the probability of detecting $(r-1)$ electrons in the interval 0 to t as given by (35) and the probability of detecting one photoelectron at time t given by (33).

$$P(r, t) = mi(t)[mU(t)]^{r-1} \exp[-mU(t)]/(r-1)! \tag{24}$$

Here the mean number of photoelectrons m is the product of the mean number of photons n and the counting efficiency η_0 and $U(t)$ is given by (36). Of particular interest is the time distribution of the first photoelectron, $P(1, t)$,

$$P(1, t) = mi(t) \exp[-mU(t)], \tag{25}$$

which for a weakly illuminated photosurface (e.g. $m < 0.1$) reduces to

$$P(1, t) = mi(t). \tag{26}$$

Equation (26) justifies the single photon statistical method where very few of the light flash photons are allowed to strike the photosurface of a photodevice. Again, the observed time distribution curve after many excitations, $P(1, t)$, traces out the shape of a constant shape, bright light flash, limited in time resolution only by the transit time fluctuations and not by the much longer impulse response, ringing, or afterpulses of the photodevice.

D'Alessio, Zampach, and Kesque (*75b*) have recently begun to explore the possibility of making fluorescence decay time measurements by eliminating the synchronous start signal and using two photodevices at the single photoelectron level as in Fig. 10. In this paper, they also consider viewing a Cerenkov light flash and so verify the method of Present and Scarl (*57*).

a. Measurements of the lifetimes of excited states of free atoms. Corney (*76*) has recently reviewed the many methods for studying the lifetimes of free atoms, molecules, and ions, including the single photon statistical technique which he considers the most accurate and widely applicable method. Figure 13 is a simplified energy level diagram of a hypothetical atom which

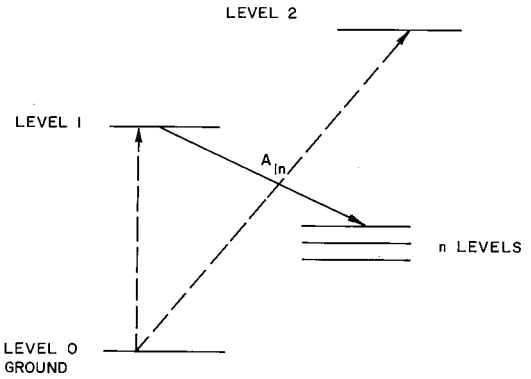

FIG. 13. Hypothetical energy level diagram of an excited state. Possible excitation modes - - - - - →. Possible decay modes ——————→.

could be part of the sample in Fig. 12. For selective excitation from the ground level to the first level, one studies the decay rate τ_1 to the various lower levels, n, using the single photon technique with either the circuit in Fig. 9 or the one in Fig. 10. In this case, the probability density function, $i(t)$, is given by

$$i(t) \sim A_{1n} N_1(0) \exp(-t/\tau_1), \tag{27}$$

where

$$\tau_1 = 1/\textstyle\sum_n A_{1n} \tag{28}$$

and $N_1(0)$ is the number of atoms excited to the level 1 at $t = 0$. A_{1n} is the transition rate for spontaneous decay from 1 to n. It has been assumed that the excitation is removed in a time short compared to τ_1 and that the source is optically thin. Collisions can shorten the decay lifetime and photon trapping effects can lengthen it so both of these phenomena can themselves be studied by this technique.

Typical lifetimes now measured by this technique range from 10 to 100 nsec and are limited by the speed of sample excitation. One excitation method is electron excitation using a pulsed electron gun with high current density, high repetition rate, and as small a spread of excitation energies as is possible. The electrical pulse that drives the electron gun is usually used as the start signal in a circuit of the Fig. 9 type and limits the time resolution to about 1 nsec. The stop signal is produced by the photodevice viewing the sample through a spectrometer of some type or an optical filter. The spectrometer is generally more useful than filters for studying wide wavelength ranges. It should have good dispersion and especially high speed since the light signal is usually not strong enough to require attenuation to single photon levels. The

weak signals mean long observation periods during which equipment stability may need to be monitored. The magnitude and fluctuation of the device noise can also become troublesome. Electron excitation can be modulated so that the digital synchronous detection method described in Section II,G,1 can be used to minimize noise. An alternate method of excitation is optical excitation by the absorption of resonance radiation. The excitation is pulsed by focusing resonance radiation from a lamp through a Kerr cell shutter. Start pulses may come from either the electrical shutter pulse or from a photodevice close-coupled to the light pulse. A lifetime of the 3^2P level of sodium has been reported as 16.6 ± 0.4 nsec using this optical excitation. The method of excitation is very selective in that only the level in resonance is excited. However, it has the following disdvantages; only intense transitions from the ground state can be studied, but those in the visible and short resonant light pulses are difficult to produce.

The experiments performed using electron excitation frequently are complicated by radiative cascades from higher levels that get excited at the same time as the one of interest. For example, the excitation cross section for level 1 may be much lower than that for level 2 in Fig. 13. If the mean energy of the electrons is beyond the threshold of level 1 by design or by necessity, level 2 can be excited and repopulate level 1 after the electron beam is turned off. Measurements on level 1 will therefore yield a decay curve consisting of a sum or difference of two exponentials with lifetimes characteristic of levels 1 and 2. A technique to overcome this complication is to view the radiation excited by the electron gun with two photodevices as shown in Fig. 12. The start signal can be a photon detected from the 21 transition by means of a suitable filter and the stop signal can be a photon detected from the 1n transition by means of another filter. The measurement thus starts when level 1 is known to be populated, but at the cost of a detection rate significantly smaller than the two previous methods. The amount and stability of the dark count becomes very important over the typical run of twenty-one hours for a measurement of the 7^3S_1 to 6^3P_1 to 6^1S_0 cascade in mercury. A 6^3P_1 lifetime of 114 ± 14 nsec was obtained. Cascades can also be selected on the basis of polarization with suitable analyzers in front of each photodevice. This last technique is limited by the spectral sensitivity of available photodevices since either the first transition is in the infrared or the second is in the ultraviolet. The increased range of spectral sensitivity mentioned in Section II,E is of interest here.

The effect of finite instrumental resolving time on the decay time measurements can be unraveled by means similar to those used in molecular and nuclear lifetime studies. In the atomic (and molecular) case, it is usually the turn-off time of the excitation that sets the limit. If one can study the decay time of an excited level with a lifetime much shorter than the instrumental

resolving time, the resulting prompt delay distribution obtained with Fig. 9 is determined solely by the characteristics of the apparatus. The observed timing distribution of the level under study is then the convolution of its true decay shape with the prompt delay shape. For electron excitation, a prompt curve has a full width at half-maximum of from 1 to 4 nsec. For lamp excitation, the prompt curve (in this case the shape of the excitation pulse) can be obtained by substituting a lamp not resonant with the level under study. The deconvolution of true decay curves from observed ones knowing the prompt delay curves is discussed in Section III,D,1,b and by Corney (*76*).

b. Measurement of fast fluorescence decay times of molecules. Fast fluorescence studies are of current interest to biophysicists and biochemists because both the fluorescent process in certain molecules can be studied as a function of their environment and certain of the fluorescing molecules can be used as a tag to study macromolecules. Fluorescence is included as a topic separate from Section III,D,1,a because of the much broader excitation and emission bands involved and the different interests of those who study it. Excitation can be done by electron beams and other techniques, but the currently popular technique is light pulse excitation. Fast decay lifetimes range from about 1 nsec to 10 μsec. Schuyler and Isenberg (*77a*) describe a recently constructed monophoton fluorometer that uses the single photon statistical technique and a pulsed light source, present examples of performance, and outline an analysis scheme that separates a multiple decay time fluoresence curve from the excitation function. Their sample geometry is similar to that shown in Fig. 12 with one photomultiplier viewing the excitation pulse at high levels and the other viewing the sample fluorescence at the single photon level, all through the appropriate filters, monochromators, and polarizers. The electronics is similar to that shown in Fig. 10, but with the start and stop channels reversed for better performance of the time-to-pulse-height converter and a single channel pulse height analyzer selecting the pulse heights of the single photon events to be analyzed. This latter selection with an RCA 8850 allows a higher data rate as discussed in Section III,C,1 without distorting the shape of the observed time distribution. The fluorescence is normally quite bright and may still need to be attenuated to an average of one photoelectron per flash. Coates (*77b*) gives a brief review of the measurement corrections for the "pile-up" error which can occur when the above selection is not made. In practice, the excitation flash need not be very short although it must have a stable shape which can be measured by the same monophoton technique. A typical light pulse triggered by a thyratron is about 7 nsec wide. The performance of their instrument was tested by measuring a lifetime of 4.00 ± 0.5 nsec for a deaerated solution of 8×10^{-5} M anthracene in benzene. Ware (*78a*) has also recently discussed the monophoton technique in his

review of transient luminescence measurements. Selinger and Ware (*78b*) have applied this technique to a study of single vibronic levels in benzene at low pressures. Halpern and Ware (*78c*) have applied it to vibrational relaxation studies in hexafluoroacetone. Finally, Tao (*79a*) describes a monophoton fluorometer used in his studies of the Brownian rotational diffusion of macromolecules in solution. He used a dye molecule as a tag and measured the decay of its fluorescence for both states of polarization after exciting it in one state of polarization. The decays are in general a combination of several exponentials and yield information about the size, shape, and other aspects of the macromolecule in solution.

The observed statistical decay curve, $F(t)$, is a convolution

$$F(t) = \int_0^t i(s)P(t-s)\,ds \tag{29}$$

of the shape of the fluorescence $i(t)$ and an instrument response function, $P(t)$. The instrument response function is itself a convolution of the system time resolution, $R(t)$, and the excitation function, $E(t)$.

$$P(t) = \int_0^t R(s)E(t-s)\,ds. \tag{30}$$

For flash lamp excitation, it is customary to measure $P(t)$ directly by removing the sample from Fig. 12. The stability of $E(t)$ often determines the measurement precision of $F(t)$ rather than $R(t)$ in this case. The problem then is to extract the shape of the fluorescence curve from (29) knowing $F(t)$ and $P(t)$. Analysis methods were originally developed for the similar problem in nuclear physics. Corney (*76*) summarizes the general method of moments which relates all the moments of $i(t)$ to the moments of $F(t)$ and $P(t)$. It helps if the functional form of $i(t)$ is known. Schuyler and Isenberg (*77a*) have outlined the solution for a sum of N exponentials and have programmed a computer to plot out both the data and desired decay curve. If the expected $i(t)$ consists of a single exponential, a number of simplified relations can be obtained for the lifetime, τ, as summarized by Corney (*76*). The most important one for these considerations is the relation

$$dF(t)/dt = [P(t) - F(t)]/\tau. \tag{31}$$

This equation can be immediately applied to the case discussed in Section III,C,2,b where the instrument response function $P(t)$ was measured and the excitation function $E(t)$ was assumed exponential. The system time resolution, $R(t)$, which depends mainly on the transit time fluctuations, can be obtained from (30) using the appropriate form of (31). Koechlin and Raviart (*71*) used this analysis in their study of photodevice transit time fluctuations with

light pulses of comparable or greater widths. A late peak in $R(t)$ with some photomultipliers is currently causing problems in fast fluorescence experiments and is described by Stevens and Longworth (*79b*).

The single photon statistical technique of measuring decay curves was first applied to bright fluorescence decays by Bollinger and Thomas (*74*) who were interested in the shape of the decay at long times in organic scintillators. These shapes depend on the mode of excitation (here different nuclear particles) and allow one to discriminate against detection of unwanted decay particles. Yates and Crandall (*73*) measured the decay curves of fifteen scintillators for incident gamma rays, finding Naton 136 to have a short decay time of 1.9 nsec. Miehe *et al.* (*75a*) in an extension of (24) show theoretically and experimentally that the data rates in these measurements can be notably improved by not only selecting actual single photoelectrons but by timing the first photoelectron when two, three, or more are detected. Scintillators are also used as the first element in the photodevice channel of experiments to measure nuclear (or particle) lifetimes or particle velocities as discussed in Section III,D,1,d. If their fluorescence decay were initiated instantaneously by the incident particle, the instrument response function, $P(t)$, would be due entirely to the photodevice time resolution (here the resolution at multiphoton levels) in the manner of (30). However, the decay is not initiated instantaneously and the finite transfer times of the excitation energy will also limit the precision of measurement of a nuclear decay time. These growth times in the scintillator have been studied with the monophoton method by Koechlin and Raviart (*71*) who later found a rise time of 0.8 nsec and fast decay time of 1.6 nsec for Naton 136. Fast scintillators are not, therefore, particularly useful for providing fast light pulses to measure the transit time fluctuations of photodevices.

c. Measurements of lifetimes of relaxed excited states of color centers. Bosi, Bussolati, and Spinolo (*79c*) have used the monophoton technique to study lifetimes of F, M, and R centers in alkali halides. Lifetimes in the range of 20 nsec were obtained to accuracies of 1 nsec and concentration and temperature dependences studied. Cova, Bussolati, and Bertolaccini (*79d*) describe the technique.

d. Measurements of lifetimes of excited states of nuclei. Measurements of the lifetimes of excited states of nuclei are usually made by examining a radiative cascade in detail. For example, the beta ray from the decay of ^{207}Hg provides the start signal in a circuit similar to Fig. 10 and the gamma ray from an excited state of ^{203}Tl provides the stop signal by means of the light flashes they produce in organic scintillators coupled to the photodevices. The energies of the decay products are selected by a slow, linear channel from each photomultiplier. Both of the photomultipliers are closely coupled to the scintillators at a level of 30 or more photoelectrons released from their

photosurfaces per flash in order to improve the time resolution. The single photon transit time fluctuations (13) can be expected to be improved by the square root of the number of photoelectrons released due to better sampling of the KS1 region. Schwarzschild (*80*) reviews these techniques and quotes 281 ± 60 psec for the lifetime of the 279 keV decay of ^{203}Tl. The lifetime is, of course, the slope of a curve each point of which has considerably more uncertainty. The decay curve is determined from the observed curve as discussed in Section III,D,1,b by observing a prompt delay distribution using the gamma rays of ^{60}Co for example. The two-channel, prompt decay time resolution is typically 0.2 nsec for close-coupled photomultipliers and gives an indication of the start channel jitter in the measurement of scintillator growth and decay times. Meiling and Stary (*3*) also review these nuclear applications.

The use of scintillators adds further uncertainties to the decay time measurements above those discussed for the other applications. Not only are there the growth and decay times of the fluorescence pulse involved, but also problems due to the need to collect a large amount of the fluorescence on the photosurface and the resultant need for large photosurfaces. If the growth time, the collection time spread, and the transit time fluctuation were zero, if the walk effect were eliminated, and if the initial fluorescence decay were a simple exponential, it is clear that the scintillation should be as bright as possible and the timing discriminator trigger level as low as possible so that one could detect the passage of the nuclear particle at that very instant. The trigger level is thus set near the single photoelectron level even though the whole flash seen by the photodevice may produce an average of m electrons. The discriminator should also be blanked after this detection until the flash has decayed. The uncertainty in time for the appearance of the first C photoelectrons has been shown to be

$$\varepsilon_t = \tau\sqrt{C/m}, \qquad m \gg C \tag{32}$$

in this simple case. For a fast scintillator, $\tau = 2$ nsec and $m = 20$ or larger, so that $\varepsilon_t = 0.1$ nsec for $C = 1$. Before this limit is reached, one must take into account all the effects assumed negligible. The recent state of the theory which includes all these effects and tries to explain the prompt delay curves as a function of trigger level is summarized by Donati *et al.* (*12*). The beginner may wish to read an earlier paper first (*52*). It is this terminology and theory that has been followed in this review, at least for the photodevice analysis. Until one knows the growth time and the transit time fluctuations for the particular experiment, application of the theory requires assumptions as to values and shapes, prediction of a prompt decay curve, and a comparison with experiment which hopefully yields unique values for these two unknowns. Present, Schwarzschild, Spirn, and Wotherspoon (*81*) measured a

prompt delay curve with width of 0.2 nsec using Naton 136 with $m = 100$, an Amperex XP1020, and pulse height selection channels. This optimum instrumental resolution occurred at a trigger level of 10 photoelectrons and appeared to be fundamentally limited by the growth time of the light pulse in the scintillator rather than transit time fluctuations or (32). Bertolini, Cocci, Mandl, and Rota (*82*) found a prompt decay curve time resolution of 164 psec using an XP1020. Miehe *et al.* (*62*) found a prompt decay curve time resolution of 185 psec using an RCA C70045. Both of these measurements were with a ^{60}Co source and a Naton 136 scintillator producing multiphoton signals. Short light pulsers are also used in this measurement and typically give better time resolutions. Miehe *et al.* (*62*) obtained 76 psec with the C70045. Decay lifetimes of nuclear states less than the width of the prompt delay curve cannot be measured by this technique.

2. *The Lunar Laser Ranging Experiment*

Accomplishment of the scientific objectives of the Lunar Laser Ranging Experiment which are listed in Table VI required that the light travel time between the earth and the moon be determined daily over an extended period of time to an accuracy of 1 nsec or better whenever the moon was up (*83*). The experiment became possible when man could bring a "point" retroreflector to the moon. The systems design of the experiment which included practical retroreflector arrays, one of the world's largest telescopes,

TABLE VI

SCIENTIFIC OBJECTIVES OF THE LUNAR LASER RANGING EXPERIMENT[a]

Lunar orbit[b]	Mean distance
	Eccentricity
	Angular position of moon
Selenophysics[b]	Physical libration parameters[c]
	Coordinates of arrays w/r center of lunar mass
Geophysics	Short term fluctuations in rotation period of earth
	Station distance from earth rotation axis
	Station distance from equatorial plane[b]
	Motion of pole[b]
	East–west continental drift rate[b]
	Drift of Hawaii toward Japan
Gravitation and relativity	Equivalence principle for gravitational self energy

[a] Significant improvement is expected in all parameters here listed.
[b] Three or more observing stations are required.
[c] Three or more retroreflectors are required.

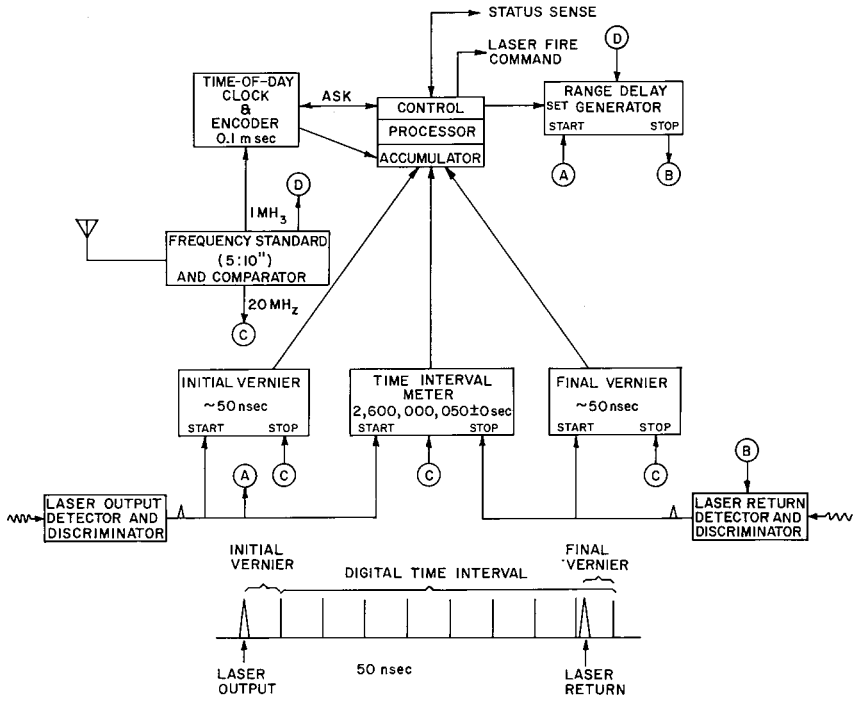

FIG. 14. Representation of the nanosecond-resolution time-interval measurement system at the McDonald Observatory Lunar Ranging Station. Special logic circuits eliminate any ± 1 count uncertainty in the digital interval. The verniers are time-to-pulse-height converters. From Alley *et al.* (*83*). (Copyright 1970 by the American Association for the Advancement of Science.)

and a narrow beam, nanosecond-pulse laser indicated that less than one photoelectron would be released at the photodetector per laser firing under average conditions. The nominal round-trip travel time of a pulse of light to the moon and back is 2.5 sec. The problem of measuring this interval precisely was solved as indicated in Fig. 14 by counting a 20 MHz standard clock signal from a start light pulse to a stop light pulse. At each end of this interval, a time-to-pulse-height converter was linked so that it measured the time (about 50 nsec) between a clock pulse and the relevant light pulse, but so that no extra clock pulses were counted. Operation under the varying and often difficult background conditions required that a narrow time gate (e.g. 6 μsec) be opened at the expected arrival time in addition to requiring a 6 arcsec spatial filter and a 0.7 Å spectral filter. The laser firing rate of 20 ppm and the rapid change of travel time due to earth rotation required an on-line central computer which programmed the gate generator (among other

control duties) and which was then used to record the data. The lunar ephemeris that was used in the prediction of the gate opening time itself was accurate to about 1 μsec. An accurate time-keeping terminal was provided which also served to monitor the 20 MHz rate. A recent description of the McDonald Observatory station is available (*84a*), as is a more complete discussion of the role of single photon detection and timing in the experiment (*84b*).

Figures 15 and 16 display a 50 laser-firing run with 12 individual returns which is an above average return. Figure 15 shows the return in 50 nsec blocks as a function of range time relative to the range time predicted by the ephemeris. The run was at night, but during bright moon and so shows random noise counts. Figure 16 examines ten returns in the 50 nsec block as a function of epoch of arrival. The returns are due to single photoelectrons released at the photocathode of the photodetector. The uncertainty of each event is shown as ± 2 nsec due to the present laser pulse width of 4 nsec. The return photons were detected at about 0.5% total receiver efficiency based on an RCA C31000F photomultiplier and their arrival time determined by an Ortec 270 constant-fraction-of-pulse-height timing discriminator. Given

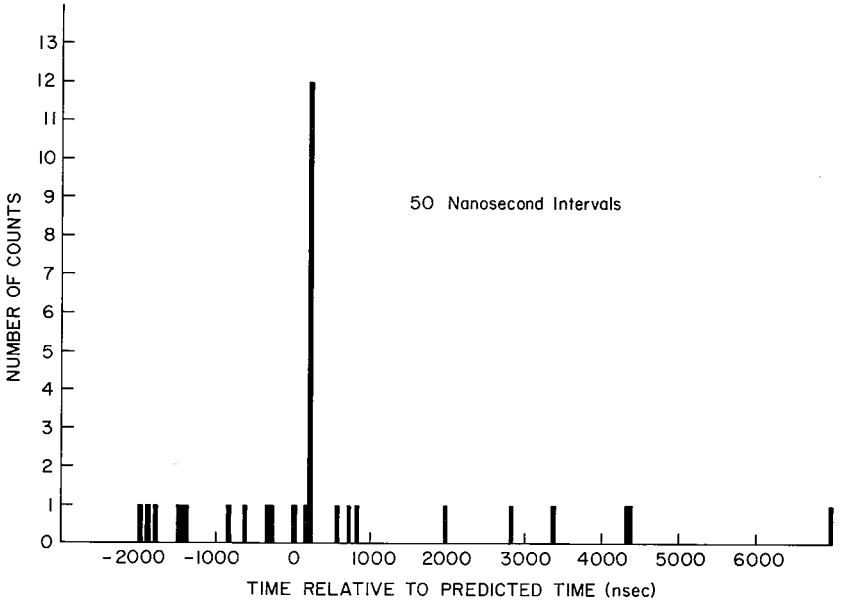

FIG. 15. Histogram of 12 lunar returns of a fifty laser shot run on 1970 day 075 starting at 04:57 U.T. from McDonald Observatory. Abscissa is range time relative to that predicted in 50 nsec intervals. Random counts are due to high background conditions. Currie (*85*) (Courtesy I.A.U. and Reidel Publishing Co., Dordrecht, Holland.)

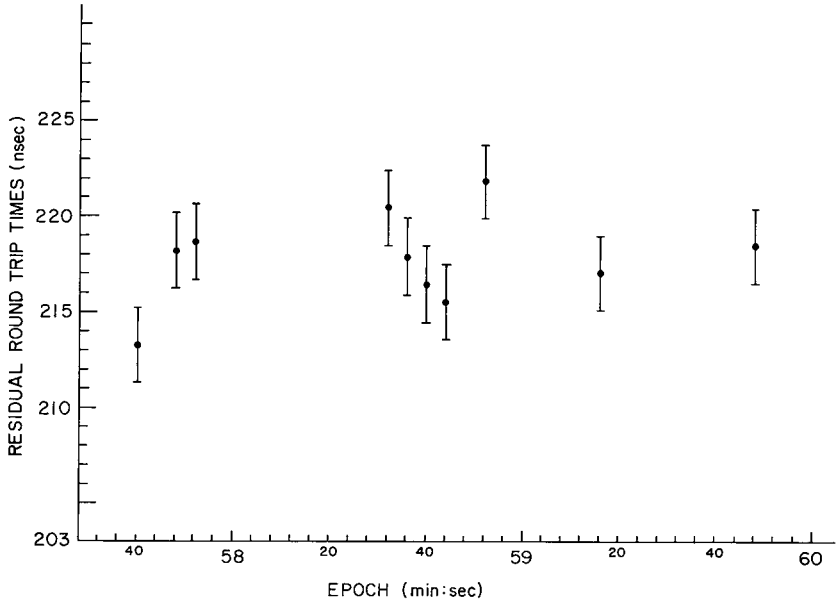

FIG. 16. Residual round trip travel times of the ten lunar returns as a function of epoch of arrival. The returns are due to single photoelectrons. The uncertainty of each event is shown as ± 2 nsec due to the present laser pulse width of 4 nsec. Residual is observed range minus calculated. Currie (*85*). (Courtesy I.A.U. and Reidel Publishing Co., Dordrecht, Holland.)

that the moon moves slowly in time over these short periods, a number of returns can decrease the uncertainty below the ± 2 nsec. The statistics of this run support a precision of ± 1 nsec which is still larger than that inherent in this particular photomultiplier. Both timing precision and accuracy are checked internally using the methods and the triggerable light pulser as discussed in Section III,C,3. A series of daily measurements will yield the minimum range and its epoch of occurrence over an extended period. Harmonic analysis of this range time series will permit the determinations of the quantities listed in Table VI with significant improvements over present knowledge. In some cases, three or more observing stations are required. In other cases (e.g. physical librations), three separate retroreflectors are required. Three U.S. retroreflectors are now fixed in position having been carried to the moon by Apollos 11, 14, and 15. Future range measurements using the planned subnanosecond laser transmitter will be limited in precision by the time resolution of single photon detection devices.

IV. Single Photon Detection with Moderate Timing Requirements

A number of experiments including some of the types discussed in Section III,D require only moderate timing while still requiring single photon detection. In the first class of experiments with moderate timing requirements, a pulsed or modulated source provides a sync signal to start the time interval and so aids in noise discrimination. The second class of experiments measures either directly or indirectly the distribution of arrival times of photons from light sources and is generally referred to as photon statistics or photon counting statistics experiments.

A. Experiments with Modulated Light Sources

The discussion of photometry and spectrophotometry in Section II,G showed that there were advantages in effectively modulating the weak continuous source and in detecting in synchronism with this effective modulation. The synchronous detection scheme allowed separation of signal from noise in a straightforward procedure. The many experiments with modulated sources discussed in Section II,G should strictly have been discussed here. Only one more such experiment will be mentioned, mainly because it is in an entirely different area of physics. Koons and Fiocco (*86*) measure the electron density and temperature in a low density reflex discharge in helium by Thomson scattering of cw argon-ion laser radiation at 4880 Å. An analog synchronous detection scheme was used to distinguish the scattered radiation from all other radiation entering the detector. A tunable, 1.58 Å wide interference filter was used to measure the Doppler-broadened scattered radiation as well as discriminate against the background from the plasma and laser. The background count rate was 10^5 counts/sec whereas the peak Thomson scattered intensity was equivalent to 64 counts/sec. Integration times were not quoted although error bars of about 10% appear in the data displays. The intensity of the scattered light leads to the electron density and the spectral broadening to the temperature.

Closely related to these modulation time signature methods are experiments using pulsed light sources. The pulsed light source may be used as an optical radar viewing an extended medium where one is interested in the arrival time of a very weak return in the presence of noise. Repeated flashes then build up the certainty and precision of a return from a certain distance. For example, optical probing of the upper atmosphere combines single photon detection in a height resolution element with the identification of that height element by time of flight techniques. The detection schemes discussed in Section II,D need to be supplemented by timing circuits of moderate

capabilities. Returns are normally assigned to resolution elements of about 13 μsec in width (i.e. 2 km in altitude). A single time interval meter (i.e. counting of a gated clock pulse) would waste much of the return from one flash and so workers use a digital bin sorting system or a multistop time-to-pulse-height converter in order to detect single photons from more than one altitude per flash with the same photodevice. The time-to-pulse-height converter would have much longer ranges and lower precisions than the one discussed in Section III,B. Kent and Wright (*87a*) review the aims, techniques, and results of such optical probing of the upper (and lower atmosphere). By recording the back-scattered photons from a pulse of laser light propagating toward zenith, one can measure molecular densities to 80 km to a few percent in about an hour at night with a height resolution of 2 km using typical Q-switched lasers operating at several pulses per minute and using large receiving mirrors (i.e. 10 m^2). Precision is shot noise limited up to about this altitude for 10 Å or narrower spectral filters and milliradian fields of view. Night sky background and/or photodevice dark counts begin to limit the precision above these altitudes. Accuracy is limited by calibration problems, the presence of aerosols, and the presence of laser light noise. Poultney (*87b*) reviews this last problem and suggests methods to eliminate it. Part of the problem comes from enhanced photodevice noise due to the intense initial light pulse. If opaque shutters cannot be used in these laser excitation experiments, only careful selection of optical components and photodevices can reduce the enhanced dark noise.

B. Photon Statistics Experiments

1. Introduction

Measurement of photon statistics is the determination of the arrival times of photons from a source by the measurement of the distribution of photoelectrons detected. The former distribution can be directly related to the latter. Photon statistics experiments can thus characterize the statistical properties of a light beam or, if these are known, yield information about the internal behavior of various statistical media which scatter that beam. Two active workers in this field, Pike (*88*) and Arecchi (*89*), give recent reviews of photon statistics theory and experiment. The origin of these statistical properties and the scope of their application can be obtained from the following picture. Illuminate a photosurface with a light beam of constant intensity from an ideal laser. The probability of detecting a photoelectron in an ideal photodevice in a short time interval is a constant proportional to the constant intensity and does not depend on the time of the measurement. In other words, the photoemission process takes place completely at random in time

with no correlation between adjacent events (i.e. a Poisson distribution). Now let the laser beam scatter from a medium undergoing statistical fluctuations in some property. For example, consider micron-size particles undergoing Brownian motion in a liquid. The beam incident on the photosurface will now include different Dopper-shifted frequencies and will fluctuate in intensity due to the beating together of the various components. The intensity fluctuations in turn cause an increase in the probability of photoelectron detection at some times and a decrease at others. This variation leads to a departure from randomness of the time distribution of photoelectrons. The departure can be measured either by recording the distribution of times between events or by examining the fluctuation of counts obtained in various length counting intervals. The time scale of bunching in time or of increase in counting variance gives information about the relative motion of the particles. Its inverse is a measure of the spectral broadening of the scattered laser line. In most cases, this broadening is too small to be measured by the spectrophotometric methods described in Section II,G (e.g. 1.6 KHz linewidth corresponds to a time scale of 0.17 msec).

Similar intensity fluctuations and nonrandom photon statistics are present for laser light scattered from a medium whose dielectric constant is fluctuating for some physical reason. The physical reason can be injected from the outside as with a sound wave or it can be spontaneous due to natural thermal excitations. The spontaneous excitations can be either propagating, as in the case of optical and acoustic phonons which yield Raman and Brillouin scattering respectively, or nonpropagating as in the case of thermal density fluctuations at constant pressure which yield Rayleigh scattering. In the propagating case, there is both a lineshift which is that measured by spectrophotometry and a linewidth related to relaxation processes which is better measured using photon statistics or its equivalent. The width of the Rayleigh line in pure fluids and liquid mixtures is determined by diffusive processes; the thermal diffusivity for simple fluids and the diffusion constant for mixtures. In the normal fluids, the Rayleigh linewidth is characteristically less than 10^8 Hz. There is a great deal of current interest in the behavior of this linewidth in the vicinity of a critical point where the linewidth quickly falls to 10^5 Hz or less. It should be pointed out here that a study of the power spectrum of the fluctuating photodevice current can also provide the above information about the medium and in fact is the currently favored method (*90*). That the power spectrum can provide this linewidth information is due to the Gaussian nature of the light fields scattered by the thermodynamic fluctuations and the resultant circumstance that all correlation functions in time of order higher than the first can be expressed in terms of the first. The power spectrum involves a second-order correlation function. Degiorgio and Lastovka (*91*) compare these two approaches to intensity-correlation

spectroscopy for Gaussian fields with the uncertainty in the linewidth as the criterion. The added promise of photon statistics measurements is that they will allow the measurement of the higher order correlation functions which must be known to describe nonGaussian scattered light. The statistics of scattered light near the critical point of a medium might be expected to be non-Gaussian (*92*), due to the presence of higher order density correlations.

An ideal laser beam is itself a nonGaussian field. Photon statistics measurements have been used extensively to study the stationary and the transient statistical properties of real lasers both above and below threshold (*89*). The ideal laser beam can be transformed to a Gaussian beam by the linear scattering from a medium made of uncorrelated, statistically distributed scatters (e.g. the Brownian particles as above). The same chaotic beam can be expected from a thermal light source. A measurement would show non-Poisson statistic on time scales much shorter than the inverse linewidth. However, the narrow linewidths are more characteristic of scattered laser light than thermal light. A filtered mercury lamp with a spectral width of 1.6 GHz (i.e. 0.01 Å) would have a correlation time equal to 0.16 nsec. Such a timing precision is nearing the limit of photomultipliers while the linewidth can be easily measured by spectroscopic means. The measurement of the photon statistics of a thermal source was made as a check on the theory in this case and is here discussed in Section IV,B,3 rather than in Section III,D. The reason that typical thermal sources yield Poisson detection statistics is that the fluctuations occur on an extremely short time scale and so are not seen by any detector. Most applications of photon statistics measurements will be in the longer time domains (e.g. microseconds).

2. *Theory of Photon Statistics Experiments*

Consider a photodevice illuminated by polarized light of intensity $ni(t)$. The probability of detecting one count in the interval between t and $t + dt$ is given by

$$P(1, dt, t) = \eta_0 n\, i(t)\, dt, \tag{33}$$

where η_0 is the total counting efficiency, n is the mean rate of photons, and $i(t)$ is the normalized time dependence of the light intensity of the source. The probability that a second count is detected in the interval $t + T$ and $t + T + dt$ is given by

$$P(1, dt, t{:}\, 1, dt, t + T) = \eta_0{}^2 n^2 i(t) i(t + T)\, dt\, dt. \tag{34}$$

If $i(t)$ is constant (i.e. an ideal laser), the probability of detecting one count in any interval is a constant (33) and the probability of detecting two counts separated by any interval T is also a constant (34). These are the properties

of a random, Poisson distribution of counts in time. The joint probability (34) is not normally observed although observations could be made with a large number of coherently illuminated photodevices and timing circuits for a time t to $t + T$. If $i(t)$ is a fluctuating, stationary field, then repeated measurements with a single photodevice can be made. An ensemble average of (34) normalized by an ensemble average of (33) gives the probability of detecting two counts separated by an interval T. At T much greater than a correlation time of $i(t)$, this probability is a constant as before and the counting statistics are Poisson. At T much smaller than a correlation time, this probability is found to be doubled and the counting statistics deviate from Poisson. The ensemble average of (34) is itself not directly measured in general. If a single timing device like a time-to-pulse-height converter is used, not all T may be accessible when the counting rate in the stop channel is high. In addition, dead times in both start and stop channels can be a problem. Davidson and Mandel (*93*) deal with these issues and the above discussion in detail. A measurement of this second-order correlation gives only a measure of the source linewidth and is equivalent to spectral and power spectrum measurements. The intensity time correlations can alternately be measured using analysis of the linear photodevice signals (*89*). It is also possible to view different portions of the source and so study spatial correlation effects.

Another way of examining the detection statistics of photoelectrons is to study the fluctuations in counts for fixed counting intervals, T. The time dependent probability $P(r, T, t)$ of obtaining r counts in the interval t to $t + T$ can also be built up from (33) (*94*), and equals

$$P(r, T, t) = [mU(t)]^r \exp[-mU(t)]/r!, \tag{35}$$

where

$$U(t) = \int_t^{t+T} i(\beta)\, d\beta. \tag{36}$$

Here m is the mean count rate or total counting efficiency η_0 times the incident light intensity in photons, n. If $i(t)$ is a constant as for an ideal laser, (35) reduces to

$$P(r, T) = (mT)^r e^{-mT}/r!, \tag{37}$$

which was used in slightly different form as (20) and which is also true for a broadband thermal source. Again, $P(r,T, t)$ is not directly observable with a small number of viewing channels at one time t. If $i(t)$ is a fluctuating, random function then $P(r, T)$ can be found by taking a time or ensemble average. This operation does not, in general, preserve the Poisson form of (35) and again the fluctuations of $i(t)$ lead to a departure from Poisson counting statistics. Since no explicit closed expression for the probability distribution of U is available, the connection between an observed counting distribution, $P(r, T)$, and the field distribution, $P(U)$, is made through the normalized

factorial moments of the distributions. At times short compared to a correlation time, $P(U)$ becomes $P(i)$ which is the photon distribution. Many of the moments of $P(i)$ can be measured in this manner although not their time behaviors. The first moment is just the mean mT. The second is related to the variance of the counting statistics and involves an intensity correlation similar to (34). For a weak, Gaussian source, the normalized factorial moment equals one for T much longer than the correlation time of the fields and two for T much shorter. Thus a single counting channel could also be used to measure the linewidth of the source by varying the counting interval T. The variance itself would go from mT at long T to $mT(1 + mT)$ at short T.

3. *Photon Statistics Experiments*

Considered below are four separate photon statistics experiments: a study of spheres in Brownian motion using the counting interval method, a study of macromolecules in Brownian motion using a counting correlation method, a determination of the arrival time correlation curve of a thermal source using the methods of Fig. 10, and measurements of photodevice noise using several correlation methods. One of the first types of photon statistics experiments was the investigation of various sources and scattered light using the counting interval method. A relevant example here is the study of the statistics of laser light scattered by a dilute solution of monodisperse, micron-size spheres performed by Arecchi *et al.* (*95*). After verifying that the angular distribution of the time average of the scattered intensity was that of a single sphere and that the scattered-light spectrum was Lorentzian with the expected width (e.g. a few Hz) as obtained by the power spectrum method, this group investigated the counting statistics in an interval, T, much shorter than a coherence time. A 56 AVP photomultiplier was used with a single channel analyzer and rate meter which had a T variable from 1 to 100 μsec. The nonlinear detection circuit introduced a deadtime of 20 nsec and could distort the variance for short T and high count rates. Here the count intervals are much larger than the deadtimes (e.g. 10^4). The photocathode was reduced electrostatically to 1 mm^2 and contributed a negligible 100 counts/sec. The counting statistics for this short T were as expected (i.e. Bose Einstein) with a value of 2 for the normalized second factorial moment. Jakeman and coworkers (*96*) also investigated the statistics of laser light scattered by micron-size spheres in water at room temperature over a range of T from 1 msec to 200 msec. The optical halfwidth of the scattered light was expected to be about 7 Hz so that the coherence times would be about 0.1 sec. They used the relatively slow FW130 which was cooled with a dark count of 0.5 counts/sec. A typical count rate of single electrons was 30 counts/sec. The periods be-

tween samples T were generally equal to T. The number of samples ranged from 10^4 to 10^6. Factorial moments up to the sixth order were obtained for $T = 1$ msec and agreed with factorization theory within experimental precision (3% for the fourth moment) (*88*). The halfwidth of the optical spectrum of known shape was then obtained by determining the dependence of the normalized second factorial moment of the counting statistics on the size of the counting period T. The result of fitting the measured curve with the predicted one was 9.9 ± 2.2 Hz based on 10^4 samples.

While the counting interval method is quite convenient for determining the moments of $P(i)$ for T much less than the coherence time of the source, it can lead to difficult interpretation problems at the longer T needed to obtain the time evolution of the field and the optical linewidth. One solution is to correlate two short counting intervals separated by a variable delay (*89*). The joint counting distributions can be stored in a multichannel analyzer which reads the rate meters of each of the photodevices. The results provide at least as much information as the counting interval method and are much easier to interpret. Here one must balance ones goals against the cost of correlating equipment. Pike (*88*) describes the full time correlation of a photodevice output performed by clipping the output and autocorrelating it with itself or crosscorrelating it with its unclipped value. This clipped correlation method was applied to the measurement of the optical linewidth of laser light scattered from protein molecules undergoing Brownian motion in aqueous solution. This motion (hence linewidth) is controlled by the translational diffusion coefficients of the bovine serum albumin under study. An accuracy of 2% was obtained in the linewidth with a count rate of 200 counts/sec over a one-hour period. The effect of varying the protein concentration over a wide range could be determined in an experimental time equivalent to just one linewidth measurement by the power spectrum technique. The linewidth was shown to be a function of the pH of the buffer solution for a given concentration of serum, Fig. 17, and the molecule can be seen to "uncurl" as the pH is reduced. These experiments involve a second-order intensity correlation function, $g^{(2)}(\tau)$, where τ is the delay introduced in the correlation.

The third type of experiment is the timing of the arrival of photons from the source. The example will be the measurements on a thermal source which was mentioned in Section III,C,2,c and which made use of the method of Fig. 10 (*68*). This method is very important for short coherence times (less than 10 nsec) where it also becomes necessary to use separate photodevices. The light beam from the source is split and both devices view the same spatial coherence area. The light source was a mercury lamp filtered so that only the 4358 Å line in one polarization was observed. The linewidth was measured spectroscopically to be about 1.6 GHz or 0.010 Å. The photons were detected by two RCA 8575 photomultipliers and the delay in Fig. 10 adjusted to place

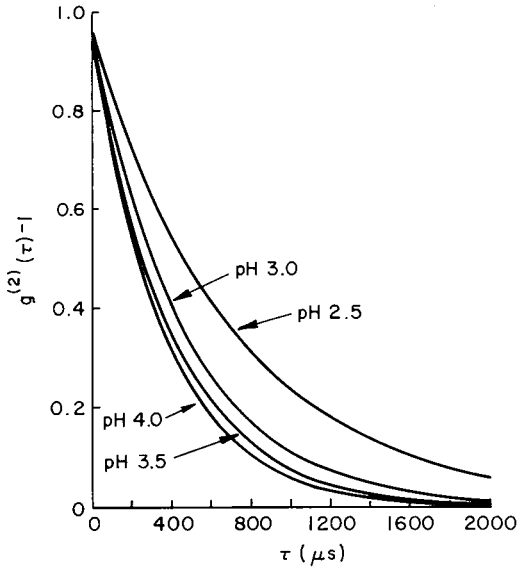

FIG. 17. The effect of changing pH on the diffusion constant (hence size) of the protein bovine serum albumin. The width of the second-order correlation function $g^{(2)}(\tau)$ is proportional to the diffusion constant. Pike (*88*). (Courtesy of Scottish Universities Summer School.)

zero delay in the center of the display range. The single, noise, and coincident rates averaged about 15 kcounts/sec, 300 counts/sec, and 4 counts/sec respectively. The time resolution of the system has an important effect on the interpretation of the experiment and was measured using a Cerenkov source as discussed in Section III,C,2,a. Figure 18 shows the result of an accumulation period of 170 hr. The theoretical shape of the time correlation curve is also shown. The time resolution and stability of the electronics was better than 0.2 nsec. The complications discussed by Davidson and Mandel (*93*) did not enter since the average time interval between events was much longer than the time difference of interest. This time difference was limited to 30 nsec by auxiliary circuits. It is the inverse of this measurement that was proposed in Section III,C,2,c as a means of determining the transit time fluctuations of fast photodevices.

Finally, these same techniques can be used to study the question of time-correlated noise in photodevices. Oliver and Pike (*23*) used the counting interval method to investigate the photoelectron statistics when an FW-130 was illuminated with laser light and found them to be very close to Poisson for T from 70 nsec (the system dead time) to 100 msec. Photodevice noise

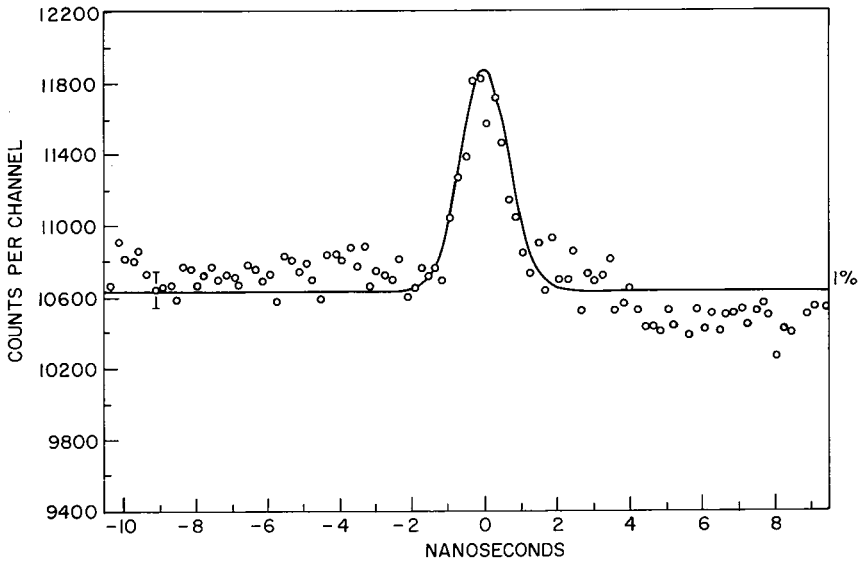

FIG. 18. Counting rate as a function of time delay between single photon detections from the 4358 Å mercury line. Light completely polarized. Accumulation time was 170 hr. From Scarl (*68*). (Courtesy of American Institute of Physics.)

counting distributions were then taken at room temperature and at −25°C. Correlations at room temperature were less than 1 in 10^4 and cooled less than their measurement limit of 1 in 10^2. For times less than 70 nsec, the impulse response showed no evidence of bunching in real time. Other photomultipliers show a different behavior (*22*). Alternately, one could determine the arrival time distributions of signal and noise using the circuit of Fig. 9 with the change that the photodevice feed both start and stop channels. For laser or wideband illumination, the distribution should be flat as in the wings of Fig. 18. The light probably would have to be attenuated so that high efficiency detection is not essential. It is at the low signal rates that the use of a time-to-pulse-height converter has advantages over the other techniques. The corrections discussed by Davidson and Mandel (*93*) may also have to be applied. The question of correlations in times shorter than device dead times would have to be answered by viewing the pulse in real time.

Appendix: Summary of Photomultiplier Notation

G_1	total gain
h	average electron transit time
$P = 2.36\lambda$	FWHM of anode current pulse (assumed Gaussian)
g	dynode multiplication factor
ε_A^2	relative amplitude variance of anode pulse
$\Delta = 2.36\,\varepsilon_A$	FWHM of SER amplitude distribution
ε_g^2	relative amplitude variance of the gain of a dynode
g_1	first dynode multiplication factor
η	photosurface quantum efficiency
η_0	total quantum counting efficiency
N_d	device dark noise rate
$R = 2.36\,\varepsilon_{PH}$	single photoelectron time resolution (assumed Gaussian)
ε_{ij}	electron transit time fluctuations, KM between cathode and multiplier, SS between dynodes, MS in multiplier, and MA between multiplier and anode
W_n	energy of electron emission from electrode
φ	interelectrode (or total) potential
s	interelectrode spacing
ε_t^2	time derivation variance
T_r	risetime of anode current pulse

Acknowledgments

I wish to thank my many colleagues for their help in the preparation of this review; especially D. Scarl, D. Currie, and D. Persyk. This work has been partially supported by NASA Grants NGR 21-002-211 and NGR 21-002-285. I also wish to express my appreciation to the University of Maryland and to C. O. Alley in particular for having made the opportunity for this study available.

References

1. E. Kowalski, "Nuclear Electronics." Springer-Verlag, Berlin and New York, 1970.
2. I. Lewis and F. Wells, "Millimicrosecond Pulse Techniques." Pergamon, Oxford, 1959.
3. W. Meiling and F. Stary, "Nanosecond Pulse Techniques." Gordon & Breach, New York, 1968.
4. RCA Staff, "Photomultiplier Manual," Tech. Ser. PT-61. RCA, Harrison, New Jersey, 1970 (See also PT-60, 1963.)
5. G. Pietri and J. Nussli, *Philips Tech. Rev.* **29**, 267 (1968).
6. J. Sharpe, "Nuclear Radiation Detectors." Methuen, London, 1964.
7. G. Morton, *Appl. Opt.* **7**, 1 (1968).
8. H. Melchior, M. Fisher, and F. Arams, *Proc. IEEE* **58**, 1466 (1970).
9. R. Simon and B. Williams, *IEEE Trans. Nucl. Sci.* **NS-15**, No. 3, 167 (1968).
10. O. Hachenberg and W. Bauer, *Advan. Electron. Electron Phys.* **11**, 413 (1959).
11. H. Krall, F. Helvey, and D. Persyk, *IEEE Trans. Nucl. Sci.* **NS-17**, No. 3, 71 (1970).
12. S. Donati, E. Gatti, and V. Svelto, *Advan. Electron. Electron Phys.* **26**, 251 (1968).
13. F. Lombard and F. Martin, *Rev. Sci. Instrum.* **32**, 200 (1961).
14. G. Morton, *Advan. Electron. Electron Phys.* **4**, 69 (1952).
15. G. Morton, H. Smith, and H. Krall, *IEEE Trans. Nucl. Sci.* **NS-16**, No. 1, 92 (1969).
16. L. Heroux, *Appl. Opt.* **7**, 2351 (1968).

17. W. Wolber, *Res./Develop.* **19**, 18 (1968).
18. L. Harris, *Rev. Sci. Instrum.* **42**, 987 (1971).
19. M. Zatzick, *Res./Develop.* **21**, 16 (1970); see also *Electro-Opt. Sys. Des.* **4**, No. 6, 20 (1972).
20. J. Boutot and G. Pietri, *IEEE Trans. Electron Devices* **ED-17**, 493 (1970).
21. P. Coates, *J. Phys. E* **4**, 201 (1971).
22. R. Foord, R. Jones, C. Oliver, and E. Pike, *Appl. Opt.* **8**, 1975 (1969).
23. C. Oliver and E. Pike, *J. Phys. D* **1**, 1459 (1968).
24. J. Topp, H. Schrötter, H. Hacker, and J. Brandmüller, *Rev. Sci. Instrum.* **40**, 11 64 (1969).
25. A. Sommer, "Photoemissive Materials; Preparation, Properties, and Uses." Wiley, New York, 1968.
26. R. Bell and W. Spicer, *Proc. IEEE* **58**, 1788 (1970).
27. J. Scheer and J. van Laar, *Solid State Commun.* **3**, 189 (1965).
28. A. Boileau and F. Miller, *Appl. Opt.* **6**, 1179 (1967).
29. M. Adelman, *in* "IRE Standards on Electron Tubes: Methods of Testing 1962" (G. Espersen, ed.), p. 78. Amer. Standards Ass., New York, 1962. See also supplement *IEEE Standard* No. 398, "Methods for Testing Photomultipliers," 1972.
30. R. Lakes and S. Poultney, *Appl. Opt.* **10**, 797 (1971).
31. W. Gunter, G. Grant, and S. Shaw, *Appl. Opt.* **9**, 251 (1970).
32. K. Crowe and J. Gumnick, *Appl. Phys. Lett.* **11**, 249 (1967).
33. G. Pietri, *IEEE Trans. Nucl. Sci.* **NS-11**, No. 3, 76 (1964).
34. L. Birenbaum and D. Scarl, *Appl. Opt.*, to be published (1972).
35. P. Coates, *J. Phys. D* **3**, 1290 (1970).
36. R. Jones, C. Oliver, and E. Pike, *Appl. Opt.* **10**, 1673 (1971).
37. R. Moore, *Electronics* **35**, 40 (1962).
38. F. Arecchi, E. Gatti, and A. Sona, *Rev. Sci. Instrum.* **37**, 942 (1966).
39. R. Tull, *Appl. Opt.* **7**, 2023 (1968).
40. M. Kerker, "The Scattering of Light," Chapters 7 and 8. Academic Press, NewYork, 1969.
41. D. McIntyre and J. Sengers, *in* "Physics of Simple Liquids" (H. Temperley, J. Rowlinson, and G. Rushbrooke, eds.), Chapter 11, North-Holland Publ., Amsterdam, 1968.
42. R. Smith, *Proc. Roy. Soc. Ser., A* **323**, 305 (1971).
43. B. Chu, *Annu. Rev. Phys. Chem.* (H. Eyring, ed.), **21**, 145 (1970).
44. G. Reynolds, *Advan. Electron. Electron Phys.* **28B**, 939 (1969).
45. T. Greytak and G. Benedek, *Phys. Rev. Lett.* **17**, 179 (1966).
46. J. Barrett and N. Adams, *J. Opt. Soc. Amer.* **58**, 311 (1968).
47. A. Mooradian, *Science* **169**, 20 (1970).
48. W. Hiltner, ed., "Astronomical Techniques." Univ. of Chicago Press, Chicago, Illinois, 1962.
49. R. Tull, *Appl. Opt.* **7**, 2019 (1968).
50. E. Dennison, *Science* **174**, 241 (1971). See, also, W. Metz, Science **175**, 1448 (1972).
51. G. Reynolds, *IEEE Trans. Nucl. Sci.* **NS-13**, No. 3, 81 (1966).
52. E. Gatti and V. Svelto, *Nucl. Instrum. and Methods* **43**, 248 (1966).
53. M. Birk, Q. Kerns, and R. Tusting, *IEEE Trans. Nucl. Sci.* **NS-11**, No. 3, 129 (1964).
54. G. Pietri, *IEEE Trans. Nucl. Sci.* **NS-9**, No. 3, 62 (1962).
55a. H. Krall and D. Persyk, *IEEE Trans. Nucl. Sci.* **NS-19**, No. 3, 45 (1972).
55b. Ph. Chevalier, J. Boutot, and G. Pietri, *IEEE Trans. Nucl. Sci.* **NS-17**, No. 3, 75 (1970).
56. R. Matheson, *IEEE Trans. Nucl. Sci.* **NS-11**, No. 3, 64 (1964).
57. G. Present and D. Scarl, *Rev. Sci. Instrum.* **41**, 771 (1970).

58a. R. Lakes and S. Poultney, *Rev. Sci. Instrum.* **41**, 1889 (1970).
58b. B. Leskovar and C. C. Lo, *IEEE Trans. Nucl. Sci.* **NS-19**, No. 3, 50 (1972).
59. G. Morton, R. Matheson, and M. Greenblatt, *IRE Trans. Nucl. Sci.* **NS-5**, No. 3, 98 (1958).
60. R. Miller and N. Wittwer, *IEEE J. Quant. Electron.* **1**, 49 (1965).
61. D. Gedcke and W. McDonald, *Nucl. Instrum. Methods* **58**, 253 (1968).
62. J. Miehe, E. Ostertag, and A. Coche, *IEEE Trans. Nucl. Sci.* **NS-13**, No. 3, 127 (1966).
63. W. McDonald and D. Gedcke, *Nucl. Instrum. Methods* **55**, 1 (1967).
64. R. Chase, *Rev. Sci. Instrum.* **39**, 1318 (1968).
65. R. Tusting, Q. Kerns, and H. Knudsen, *IEEE Trans. Nucl. Sci.* **NS-9**, No. 3, 118 (1962).
66. A. DeMaria, D. Stetser, and W. Glenn, *Science* **156**, 1557 (1967).
67. R. Carman, J. Reintjes, and H. Furumoto, *IEEE J. Quant. Electron.* **6**, 751 (1970).
68. D. Scarl, *Phys. Rev.* **175**, 1661 (1968).
69. H. Lami, J. D'Alessio, J. Zampach, R. Radicella, and J. Kesque, *Nucl. Instrum. Methods* **92**, 333 (1971).
70. Y. Koechlin, *C. R. Acad. Sci.* **252**, 391 (1961).
71. Y. Koechlin and A. Raviart, *Nucl. Instrum. Methods* **29**, 45 (1964).
72. H. Taylor, *Nucl. Instrum. Methods* **68**, 1960 (1969).
73. E. Yates and D. Crandall, *IEEE Trans. Nucl. Sci.* **NS-13**, No. 3, 153 (1966).
74. L. Bollinger and G. Thomas, *Rev. Sci. Instr.* **32**, 1044 (1961).
75a. J. Miehe, G. Ambard, J. Zampach, and A. Coche, *IEEE Trans. Nucl. Sci.* **NS-17**, No. 3, 115 (1970).
75b. J. D'Alessio, J. Zampach, and J. Kesque, *Nucl. Instrum. Methods* **97**, 235 (1971).
76. A. Corney, *Advan. Electron. Electron Phys.* **29**, 115 (1970).
77a. R. Schuyler and I. Isenberg, *Rev. Sci. Instrum.* **42**, 813 (1971).
77b. P. Coates, *J. Phys. E.* **5**, 148 (1972).
78a. W. Ware, *in* "Creation and Detection of the Excited State" (A. Lamola, ed.), Vol. I, Part A, p. 213. Dekker, New York, 1971.
78b. B. Selinger and W. Ware, *J. Chem. Phys.* **53**, 3160 (1970).
78c. A. Halpern and W. Ware, *J. Chem. Phys.* **53**, 1969 (1970).
79a. T. Tao, *Biopolymers* **8**, 609 (1969).
79b. S. Stevens and J. Longworth, *IEEE Trans. Nucl. Sci.* **NS-19**, No.1, 356 (1972).
79c. L. Bosi, C. Bussolati, and G. Spinolo, *Phys. Rev.* **B1**, 890 (1970).
79d. S. Cova, C. Bussolati, and M. Bertolaccini, *IEEE Trans. Nucl. Sci.* **NS-19**, No. 3, 18 (1972).
80. A. Schwarzschild, *Nucl. Instrum. Methods* **21**, 1 (1963).
81. G. Present, A. Schwarzschild, I. Spirn, and N. Wotherspoon, *Nucl. Instrum. Methods* **31**, 71 (1964).
82. G. Bertolini, M. Cocchi, V. Mandl, and A. Rota, *IEEE Trans. Nucl. Sci.* **NS-13**, No. 3, 119 (1966).
83. C. O. Alley, R. Chang, D. Currie, S. Poultney, P. Bender, R. Dicke, D. Wilkinson, J. Faller, W. Kaula, G. MacDonald, J. Mulholland, H. Plotkin, W. Carrion, and E. Wampler, *Science* **167**, 458 (1970).
84a. E. Silverberg and D. Currie, *in* "Space Research" (A. Stickland, ed.), Vol. 12. Springer-Verlag, Berlin and New York, 1972.
84b. S. Poultney, *IEEE Trans. Nucl. Sci.* **NS-19**, No. 3, 12 (1972).
85. D. Currie, *in* "Rotation of the Earth," Proc. IAU Symp. No. 48. Reidel Publ., Dordrecht, Holland, 1972.
86. H. Koons and G. Fiocco, *J. Appl. Phys.* **39**, 3389 (1968).
87a. G. Kent and R. Wright, *J. Atmos. Terr. Phys.* **32**, 917 (1970).

87b. S. Poultney, *in* "Space Research" (A. Stickland, ed.), Vol. 12, p. 199. Springer-Verlag, Berlin, 1972.
88. E. Pike, *in* "Quantum Optics" (S. Kay and A. Maitland, eds.), p. 127. Academic Press, New York, 1970.
89. F. Arecchi, *in* "Quantum Optics" (R. Glauber, ed.), p. 57. Academic Press, New York, 1969.
90. H. Cummins, *in* "Quantum Optics" (R. Glauber, ed.), p. 247. Academic Press, New York, 1969.
91. V. Degiorgio and J. Lastovka, *Phys. Rev. A* **4**, 2033 (1971).
92. V. Korenman, *Phys. Rev. A* **2**, 449 (1970).
93. F. Davidson and L. Mandel, *J. Appl. Phys.* **39**, 62 (1968).
94. L. Mandel, *Prog. Opt.* **2**, 183 (1963).
95. F. Arecchi, M. Giglio, and U. Tartari, *Phys. Rev.* **163**, 186 (1967).
96. E. Jakeman, C. Oliver, and E. Pike, *J. Phys. A* **1**, 406 (1968).